Received: Added at production | Revised: Added at production | Accepted: Added at production

DOI: xxx/xxxx

RESEARCH ARTICLE

Geometric Active Disturbance Rejection Control of Rotorcraft on SE(3)with Fast Finite-Time Stability

Ningshan Wang | Reza Hamrah | Amit K. Sanyal* | Mark N. Glauser

[1]Department of Mechanical & Aerospace Engineering, Syracuse University, NY, US

Correspondence
*Amit K. Sanyal, Department of Mechanical & Aerospace Engineering, Syracuse University, NY, 13244, US. Email: aksanyal@syr.edu

Present Address
This is sample for present address text this is sample for present address text

Summary

This article presents a tracking control framework enhanced by an extended state observer for a rotorcraft aerial vehicle modeled as a rigid body in three-dimensional translational and rotational motions. The system is considered as an underactuated system on the tangent bundle of the six-dimensional Lie group of rigid body motions, SE(3). The extended state observer is designed to estimate the resultant external disturbance force and disturbance torque acting on the vehicle. It guarantees stable convergence of disturbance estimation errors in finite time when the disturbances are constant and finite time convergence to a bounded neighborhood of zero errors for time-varying disturbances. This extended state observer design is based on a Hölder-continuous fast finite time stable differentiator that is similar to the super-twisting algorithm, to obtain fast convergence. A tracking control scheme that uses the estimated disturbances from extended state observer for disturbance rejection, is designed to achieve fast finite-time stable tracking control. Numerical simulations are conducted to validate the proposed extended state observer and tracking control scheme with disturbance rejection. The proposed extended state observer is compared with other existing research to show its supremacy.

KEYWORDS:
Geometric Control, Extended State Observer, Fast Finite-Time Stability, Unmanned Aerial Vehicle

1 | INTRODUCTION

Small-scale rotorcraft unmanned aerial vehicles (UAVs) have become increasingly popular in various applications, such as security and monitoring, infrastructure inspection, agriculture, wildland management, package delivery, and remote sensing. However, these UAVs are frequently exposed to dynamic uncertainties and disturbances caused by turbulence induced by airflow around structures or regions. Therefore, it is crucial to ensure robust flight control performance in such challenging environments, with guaranteed stability margins even in the presence of dynamic disturbances and uncertainties. To this end, this article describes robust tracking control schemes for a rotorcraft UAV under disturbances and uncertainties.

Recent research articles on rotorcraft the UAV tracking control schemes use different methods to tackle the adverse effects of disturbances and uncertainties during the flight. Torrente et al.[1] use Gaussian processes to complement the nominal dynamics of the multi-rotor in a model predictive control (MPC) pipeline. Hanover et al.[2] use an explicit scheme to discretize the dynamics for the nonlinear MPC solved by optimization. Bangura et al.[3] use the propeller aerodynamics as a direct feedforward term on the desired thrust to re-regulate the thrust command of the rotors. Craig et al.[4] implement a set of pitot tubes onto the multi-rotor aircraft to directly sense the aircraft's airspeed. With the knowledge of propeller aerodynamic characteristics, the airspeed is

then utilized to obtain the disturbance forces and torques as feedforward terms to enhance control performance. Bisheban et al.[5] use artificial neural networks to obtain disturbance forces and torques with the kinematics information of the aircraft and then use the baseline control scheme based on the work by Lee et al.[6] in their tracking control scheme design. The methods used in these research articles either need high computational efforts[1,2,5], or require precise modeling of the aerodynamic characteristics of the rotorcraft propellers[3,4], to obtain satisfactory control performance against disturbances.

A promising control technique to maintain the control performance against disturbances and uncertainties is active disturbance rejection control (ADRC), which can be traced back to the dissertation by Hartlieb[7]. In an ADRC scheme, we first obtain an estimation of the unknown disturbance from a disturbance observer (DO) or an extended state observer (ESO), and then utilize it in the control design to reject the disturbance. ADRC and ESO are formally introduced in combination in[8], where the ESO is used to obtain disturbance estimates for disturbance rejection. Other than ESO, disturbance observer (DO)[9], and unknown input observer (UIO)[10] can also give disturbance estimates for a disturbance rejection control scheme.

ADRC schemes are widely used for rotorcraft UAV control. In the research articles by Shao et al.[11], the disturbance estimation from asymptotically stable (AS) ESOs is employed to enhance surface trajectory tracking control scheme for a multi-rotor UAV in the presence of parametric uncertainties and external disturbances. Liu et al.[12] propose fixed-time stable disturbance observers (FxTSDO) and fault-tolerance mechanisms and utilize them in their translation and attitude control scheme. Mechali et al.[13] present FxTS ESOs for the same purpose. Wang et al.[14] implement incremental nonlinear dynamics inversion (INDI) control combined with a sliding-mode observer (SMO) for disturbance estimation and rejection. Jia et al.[15] employ the disturbance model obtained by Faessler et al.[16], and then estimate the drag coefficient as a parameter. This disturbance model is also employed by Moeini et al.[17]. Cui et al.[18] use an adaptive super-twisting ESO for the disturbance estimation. Bhale et al.[19] carry out disturbance estimation with the discrete-time finite-time stable (FTS) disturbance observer by Sanyal[20].

There are several methods to ensure the stability of the above-mentioned ESO/DO designs used for rotorcraft tracking control. The linear ESO by Shao et al.[11] is AS. Mechali et al.[13] use the concept of geometric homogeneity[21] to obtain a FTS ESO. A similar method is proposed in the ESO design by Guo et al.[22]. The Lyapunov functions/candidates used in the ESO stability analysis by Mechali et al.[13] and Guo et al.[22] are based on Rosier[21], and are presented implicitly. Jia et al.[15], Moeini et al.[17] and Liu et al.[12] use variants of the DO proposed by Chen[9]. Another method is to use the super-twisting algorithm (STA)[23] to obtain ESO design. Xia et al.[24] use this method in ESO design for spacecraft attitude control, and Cui et al.[18] design an adaptive super-twisting ESO using a similar method in a multi-rotor ADRC scheme.

In much of the prior literature for rotorcraft UAV attitude control with ESO/DOs for disturbance torque estimation and rejection in rotational dynamics, the attitude kinematics of the ESOs/DOs are either based on local linearization or represented using local coordinates (like Euler angles) or quaternions. Local coordinate representations can have singularity issues (e.g., gimbal lock with Euler angles), while quaternion representations may cause instability due to unwinding[25,26]. In situations where the UAVs have to carry out aggressive maneuvers, as in rapid collision avoidance for example, disturbance estimation and rejection from such schemes may not be reliable or accurate enough for precise control of the UAV.

This article presents a scheme enhanced by ESO on SE(3)for rotorcraft UAVs under complex and challenging aerodynamic environments. The ESO on SE(3) estimates the disturbance forces and torques during the flight of a rotorcraft UAV in both translation and rotation. The ADRC scheme on SE(3) then incorporates the disturbance estimation from the ESO and the feedback from tracking control schemes to drive the UAV to the desired trajectory. The ESO and ADRC schemes are fast finite-time stable (FFTS), abbreviated as FFTS-ESO and FFTS-ADRC, respectively. The tracking control module with fast finite-time stability is developed based on the research article by Viswanathan et al.[27]. The FFTS-ESO design is based on a novel Hölder-continuous fast finite-time stable differentiator (HC-FFTSD). We carry out several sets of numerical simulations to show the validity of the proposed FFTS-ESO and FFTS-ADRC schemes.

We highlight some unique contributions of this dissertation.

- The proposed ESO is the major contribution of this article. In the proposed ESO, which is the core of the proposed ADRC scheme, the pose of the rotorcraft is represented directly on the Lie group of rigid body transformations, the special Euclidean group SE(3). Unlike the ESO and DO designs reported by Mechali et al.[13], Shao et al.[11], and Cui et al.[18], which use Euler angles or quaternions for attitude representation or do not include attitude kinematics, like the DO by Bhale et al.[19] in disturbance torque estimation, the pose of the aircraft in this article is represented in SE(3)to avoid kinematic singularities. We do not use local coordinates (like Euler angles) or (dual) quaternions for pose representation so that we avoid singularities due to local coordinate representations or quaternion unwinding, as reported by Bhat et al.[25], and Chaturvedi et al.[26]. To the best of the author's knowledge, there is no existing publication on aircraft ADRC using ESO with pose representation on SE(3).

- In the FFTS-ADRC scheme, the FFTS-ESO is based on the HC-FFTSD. The commonly used geometric homogeneity method[21,22,28,29,30], cannot provide a straightforward (or explicit) Lyapunov function to prove the finite-time stability of the scheme. The (implicit) form of their Lyapunov functions is by Rosier[21]. This implicit Lyapunov function complicates the robustness analysis under measurement noise and time-varying disturbances when that analysis is essential for an ESO designed for disturbance estimation in ADRC schemes. We propose HC-FFTSD as an approach inspired by the STA[23,31] of sliding-mode control (SMC). This approach gives a straightforward design of a strict Lyapunov function, which is explicit, and therefore avoids the weakness mentioned above.
- Based on the HC-FFTSD, the proposed FFTS-ESO schemes are both FFTS and Hölder-continuous, unlike the common STA and other FTS schemes that use discontinuous methods like terminal sliding-mode. Therefore, the proposed FFTS-ESO avoids the potentially harmful chattering phenomenon[32], while maintaining FTS convergence.
- With explicit Lyapunov function in the stability analysis, we present proof of the robustness of the proposed FFTS-ESO under time-varying disturbing forces, torques, and measurement noise. To the best of the authors' knowledge, there is no prior research on the noise robustness of ESO using Lyapunov analysis.

The remainder of the article is as follows. Section 2 presents some preliminary results that are needed to obtain sufficient conditions for the stability of the ESO and ADRC schemes. HC-FFTSD is presented, along with its stability and robustness analysis in Section 3. In Section 4, the ESO and the tracking control design problems are formulated. Section 5 describes the detailed FFTS-ESO design, which is based on the differentiator design in Section 3. Section 6 obtains the control law of FFTS-ADRC for stable tracking control on SE(3) with the estimated disturbances obtained from FFTS-ESO described in Section 5. In Section 7, we present two sets of numerical simulation results to validate the proposed FFTS-ESO and FFTS-ADRC, respectively. The first set of simulations validate the proposed FFTS-ESO and compare it with other existing literature on disturbance estimation to show the supremacy of FFTS-ESO. The second set of simulations are based on the discretization provided by the Lie group variational integrator (LGVI)[33] model, FFTS-ESO for disturbance estimation, and the obtained control laws of FFTS-ADRC to validate the proposed disturbance rejection control scheme. We conclude the paper, in Section 8, by summarizing the results and highlighting directions for forthcoming research.

2 | PRELIMINARIES

The statements and definitions in this section are used in the technical results obtained in later sections. The statements given here give the conditions under which a continuous system is finite-time stable, fast finite-time stable, and practically finite-time stable using Lyapunov analysis, and the last statement is used in developing the main result.

Lemma 1 (Finite Time Stability)**.** [34] Consider the following system of differential equations,

$$\dot{x}(t) = f(x(t)),\ f(0) = 0,\ x(0) = x_0, \tag{1}$$

where $f : \mathcal{D} \to \mathbb{R}^n$ is continuous on an open neighborhood $\mathcal{D} \subset \mathbb{R}^n$ of the origin, and let there be a continuous and differentiable function $V(x(t))$ that is positive definite. Let $V(x)$ satisfy the following inequality:

$$\dot{V} \leq -\lambda V^{\alpha}, \tag{2}$$

where $x(t) \in \mathcal{D}\backslash\{0\}$, $\lambda > 0$, $\alpha \in (0, 1)$. Then the system (1) is FTS at the origin, which means $\forall x_0 \in \mathcal{D}$, x can reach the origin in finite time. Moreover, the settling time T, the time needed to reach the origin, satisfies

$$T \leq \frac{V^{1-\alpha}(x_0)}{\lambda(1-\alpha)}. \tag{3}$$

Lemma 2 (Fast Finite-Time Stability)**.** [35] Consider the system (1) and let there be a continuous and differentiable function $V(x(t))$ that is positive definite. Let $V(x)$ satisfy the following inequality:

$$\dot{V} \leq -\lambda_1 V - \lambda_2 V^{\alpha}, \tag{4}$$

where $x(t) \in \mathcal{D}\backslash\{0\}$, $\lambda_1, \lambda_2 > 0$, $\alpha \in (0, 1)$. Then the system (1) is FFTS at the origin and the settling time T satisfies:

$$T \leq \frac{1}{\lambda_1(1-\alpha)} \ln \frac{\lambda_1 V^{1-\alpha}(x_0) + \lambda_2}{\lambda_2}. \tag{5}$$

Lemma 3 (Practical Finite-Time Stable)**.** [35,36] Consider the system (1) and let there be a continuous and differentiable function $V(x)$ that is positive definite. Let $V(x)$ satisfy the following inequality:

$$\dot{V} \leq -\lambda_1 V - \lambda_2 V^{\alpha} + \eta, \tag{6}$$

with $x(t) \in \mathcal{D}\backslash\{0\}$, $\lambda > 0$, and $\alpha \in (0, 1)$. Then the system (1) is practical finite-time stable (PFTS) at the origin, which means that the solution of (1) will converge to the following set in finite time

$$\left\{ x \,\middle|\, V(x) \leq \min\left\{ \frac{\eta}{(1-\theta_0)\lambda_1}, \left(\frac{\eta}{(1-\theta_0)\lambda_2}\right)^{\frac{1}{\alpha}} \right\} \right\},$$

where $0 < \theta_0 < 1$. The settling time T is bounded above as follows:

$$T \leq \max\left\{ t_0 + \frac{1}{\theta_0\lambda_1(1-\alpha)} \ln \frac{\theta_0\lambda_1 V^{1-\alpha}(x_0) + \lambda_2}{\lambda_2},\ t_0 + \frac{1}{\lambda_1(1-\alpha)} \ln \frac{\lambda_1 V^{1-\alpha}(x_0) + \theta_0\lambda_2}{\theta_0\lambda_2} \right\}.$$

Lemma 4. [37]Let x and y be non-negative real numbers and let $p \in (1, 2)$. Then

$$x^{\frac{1}{p}} + y^{\frac{1}{p}} \geq (x + y)^{\frac{1}{p}}. \tag{7}$$

Moreover, the above inequality is a strict inequality if both x and y are non-zero.

Definition 1. Define $H : \mathbb{R}^3 \times \mathbb{R} \to \mathrm{Sym}(3)$, the space of symmetric 3×3 matrices, as follows:

$$H(x, k) := I - \frac{2k}{x^{\mathrm{T}}x} x x^{\mathrm{T}}. \tag{8}$$

Lemma 5. Let $\mu \in \mathbb{R}^n/\{0\}$ and $\alpha \in]0, 1/2[$. Consider $\mathcal{D} : \mathbb{R}^n \setminus \{0, -\mu\}$ and define $\phi(x) : \mathcal{D} \to \mathbb{R}^+$ as:

$$\phi(x) := Y(x)^{\mathrm{T}} Y(x) \text{ where } Y(x) := \|x\|^{-2\alpha} x - \|x + \mu\|^{-2\alpha}(x + \mu). \tag{9}$$

The global maximum of $\phi(x)$ is at $x = -\mu/2$.

We attach the proof of Lemma 5 in the appendix.

3 | HÖLDER-CONTINUOUS FAST FINITE-TIME STABLE DIFFERENTIATOR (HC-FFTSD)

In this section, we design the error dynamics for the proposed ESO in Section 5 in the form of an HC-FFTSD. We analyze the stability and robustness of the proposed HC-FFTSD in this section, to support the development of the ESO design in Section 5. Theorem 1 covers the stability proof of the proposed HC-FFTSD. Corollary 1 describes the convergence performance of the differentiator under external disturbances. Corollary 2 describes the convergence performance of the differentiator under measurement noise. In the analysis that follows, $e_1 \in \mathbb{R}^n$ stands for the measurement estimation error and $e_2 \in \mathbb{R}^n$ stands for the disturbance estimation error in the ESO error dynamics, respectively. In this section and the remainder of this paper, we denote the minimum and maximum eigenvalues of a matrix by $\lambda_{\min}(\cdot)$ and $\lambda_{\max}(\cdot)$, respectively.

Theorem 1. Let $p \in]1, 2[$ and $k_3 > 0$. Define $\phi_1(\cdot) : \mathbb{R}^n \to \mathbb{R}^n$ and $\phi_2(\cdot) : \mathbb{R}^n \to \mathbb{R}^n$ as follows:

$$\begin{aligned} \phi_1(e_1) &= k_3 e_1 + (e_1^{\mathrm{T}} e_1)^{\frac{1-p}{3p-2}} e_1, \\ \phi_2(e_1) &= k_3^2 e_1 + \frac{2k_3(2p-1)}{3p-2} (e_1^{\mathrm{T}} e_1)^{\frac{1-p}{3p-2}} e_1 + \frac{p}{3p-2} (e_1^{\mathrm{T}} e_1)^{\frac{2(1-p)}{3p-2}} e_1. \end{aligned} \tag{10}$$

Define the differentiator gains $k_1, k_2 > 0$ and $\mathcal{A}^* \in \mathbb{R}^{2\times 2}$, as:

$$\mathcal{A}^* = \begin{bmatrix} -k_1 & 1 \\ -k_2 & 0 \end{bmatrix}, \tag{11}$$

which makes $\mathcal{A}^*$ a Hurwitz matrix. Thereafter, the differentiator design:

$$\begin{aligned} \dot{e}_1 &= -k_1 \phi_1(e_1) + e_2, \\ \dot{e}_2 &= -k_2 \phi_2(e_1), \end{aligned} \tag{12}$$

ensures that $(e_1^{\mathrm{T}}, e_2^{\mathrm{T}}) \in \mathbb{R}^{2n}$ converges to the origin in a fast finite-time stable manner.

Proof. The proof of Theorem 1 is based on Theorem 1 by Vida et al.[31], Theorem 1 by Moreno[23] and Proposition 3 by Cruz[38]. Two properties of ϕ_1 and ϕ_2 are provided as follows.

Property 1 (P1): The Jacobian of $\phi_1(e_1)$, denoted $\phi_1'(e_1)$, is given as follows:

$$\phi_1'(e_1) = \frac{\mathrm{d}\phi_1(e_1)}{\mathrm{d}e_1} = k_3 I + (e_1^{\mathrm{T}} e_1)^{\frac{1-p}{3p-2}} \left[I - \frac{2(p-1)}{3p-2} \frac{e_1 e_1^{\mathrm{T}}}{e_1^{\mathrm{T}} e_1} \right], \tag{13}$$

so that the following identity holds:

$$\phi_2(e_1) = \phi_1'(e_1)\phi_1(e_1) \tag{14}$$

Property 2 (P2): ϕ_1' is a positive definite matrix, which means $\forall w \in \mathbb{R}^{2n}, e \in \mathbb{R}^n$,

$$0 < \lambda_{\min}\{\phi_1'(e_1)\}||w||^2 \leq w^{\mathrm{T}}\phi_1'(e_1)w \leq \lambda_{\max}\{\phi_1'(e_1)\}||w||^2. \tag{15}$$

The maximum and minimum eigenvalues of $\phi_1'(e_1)$ employed in (15) *are as given below:*

$$\lambda_{\max}\{\phi_1'(e_1)\} = k_3 + (e_1^{\mathrm{T}} e_1)^{\frac{1-p}{3p-2}}, \tag{16}$$

$$\lambda_{\min}\{\phi_1'(e_1)\} = k_3 + (e_1^{\mathrm{T}} e_1)^{\frac{1-p}{3p-2}} \frac{p}{3p-2}. \tag{17}$$

From Theorem 5.5 by Chen[39], we know that for a Hurwitz matrix $\mathcal{A}^*$ as in (11), $\forall\, \mathcal{Q}^* \in \mathbb{R}^{2\times 2}$ where $\mathcal{Q}^* \succ 0$, the Lyapunov equation:

$$(\mathcal{A}^*)^{\mathrm{T}}\mathcal{P}^* + \mathcal{P}^*\mathcal{A}^* = -\mathcal{Q}^*, \tag{18}$$

has a unique solution $\mathcal{P}^* \succ 0$. Express the positive definite matrices $\mathcal{P}^*$ and $\mathcal{Q}^*$ in components as:

$$\mathcal{P}^* = \begin{bmatrix} p_{11} & p_{12} \\ p_{12} & p_{22} \end{bmatrix},\ \mathcal{Q}^* = \begin{bmatrix} q_{11} & q_{12} \\ q_{12} & q_{22} \end{bmatrix}.$$

With $\mathcal{P}^*$ defined as the solution to (18), $\mathcal{A}^*$, $\mathcal{P}^*$ and $\mathcal{Q}^*$ can be augmented to $\mathcal{A}, \mathcal{P}, \mathcal{Q} \in \mathbb{R}^{2n\times 2n}$, as follows:

$$\mathcal{A} = \begin{bmatrix} -k_1 I & I \\ -k_2 I & 0 \end{bmatrix},\ \mathcal{P} = \begin{bmatrix} p_{11} I & p_{12} I \\ p_{12} I & p_{22} I \end{bmatrix},\ \mathcal{Q} = \begin{bmatrix} q_{11} I & q_{12} I \\ q_{12} I & q_{22} I \end{bmatrix}.$$

The augmented matrices $\mathcal{A}, \mathcal{P}, \mathcal{Q}$ defined above also satisfy a Lyapunov equation as given below:

$$\mathcal{A}^{\mathrm{T}}\mathcal{P} + \mathcal{P}\mathcal{A} = -\mathcal{Q}. \tag{19}$$

Further, the eigenvalues of $\mathcal{P}$ and $\mathcal{P}^*$, are related such that $\lambda_{\min}\{\mathcal{P}^*\} = \lambda_{\min}\{\mathcal{P}\}$, and $\lambda_{\max}\{\mathcal{P}^*\} = \lambda_{\max}\{\mathcal{P}\}$. Similar relations hold for $\mathcal{Q}$ and $\mathcal{Q}^*$. Thus, with $\mathcal{P}$ as the solution to (19), we consider the following Lyapunov candidate:

$$V(e_1, e_2) = \zeta^{\mathrm{T}}\mathcal{P}\zeta, \tag{20}$$

where $\zeta \in \mathbb{R}^{2n}$ is defined as $\zeta := [\phi_1^{\mathrm{T}}(e_1), e_2^{\mathrm{T}}]^{\mathrm{T}}$ and $\mathcal{P}$ is the augmented $\mathcal{P}^*$, which is the unique solution of (18) for a given $\mathcal{Q}^* \succ 0$. The upper and lower bounds of the Lyapunov candidate V in (20) are as given below:

$$\lambda_{\min}\{\mathcal{P}\}\,\zeta^{\mathrm{T}}\zeta \leq V(e_1, e_2) \leq \lambda_{\max}\{\mathcal{P}\}\,\zeta^{\mathrm{T}}\zeta. \tag{21}$$

From (21), we obtain the following two inequalities:

$$\lambda_{\min}\{\mathcal{P}\}\,(e_1^{\mathrm{T}}e_1)^{\frac{p}{3p-2}} \leq \lambda_{\min}\{\mathcal{P}\}\,[\phi_1^{\mathrm{T}}(e_1)\phi_1(e_1) + e_2^{\mathrm{T}}e_2] \leq V(e_1, e_2) \leq \lambda_{\max}\{\mathcal{P}\}\,[\phi_1^{\mathrm{T}}(e_1)\phi_1(e_1) + e_2^{\mathrm{T}}e_2], \tag{22}$$

$$k_3^2\lambda_{\min}\{\mathcal{P}\}\,e_1^{\mathrm{T}}e_1 \leq \lambda_{\min}\{\mathcal{P}\}\,[\phi_1^{\mathrm{T}}(e_1)\phi_1(e_1) + e_2^{\mathrm{T}}e_2] \leq V(e_1, e_2). \tag{23}$$

$V(e_1, e_2)$ is differentiable everywhere except the subspace $\mathcal{S} = \{(e_1, e_2) \in \mathbb{R}^{2n} | e_1 = 0\}$. From (12) and Property (P1), we obtain the time derivative of ζ as follows,

$$\begin{aligned} \dot{\zeta} &= \begin{bmatrix} \phi_1'(e_1)\dot{e}_1 \\ \dot{e}_2 \end{bmatrix} = \begin{bmatrix} \phi_1'(e_1)(-k_1\phi_1(e_1) + e_2) \\ -k_2\phi_1'(e_1)\phi_1(e_1) \end{bmatrix} \\ &= \mathcal{D}(e_1)\mathcal{A}\zeta, \end{aligned} \tag{24}$$

where,

$$\mathcal{D}(e_1) = \mathrm{diag}[\phi_1'(e_1), \phi_1'(e_1)] \in \mathbb{R}^{2n\times 2n},\ \lambda_{\min}\left\{\mathcal{D}(e_1)\right\} = \lambda_{\min}\left\{\phi_1'(e_1)\right\}. \tag{25}$$

With the expression of $\dot{\zeta}$ in (24), we obtain the time derivative of $V(e_1, e_2)$ as

$$\begin{aligned}\dot{V} &= \dot{\zeta}^{\mathrm{T}}\mathcal{P}\zeta + \zeta^{\mathrm{T}}\mathcal{P}\dot{\zeta} = \zeta^{\mathrm{T}}((\mathcal{D}(e_1)\mathcal{A})^{\mathrm{T}}\mathcal{P} + \mathcal{P}\mathcal{D}(e_1)\mathcal{A})\zeta \\ &= -\zeta^{\mathrm{T}}\bar{\mathcal{Q}}(e_1)\zeta.\end{aligned} \tag{26}$$

where $\bar{\mathcal{Q}}(e_1)$ is as

$$\begin{aligned}\bar{\mathcal{Q}}(e_1) &= (\mathcal{D}(e_1)\mathcal{A})^{\mathrm{T}}\mathcal{P} + \mathcal{P}\mathcal{D}(e_1)\mathcal{A} = \begin{bmatrix}\bar{\mathcal{Q}}_{11}(e_1) & \bar{\mathcal{Q}}_{12}(e_1)\\ \bar{\mathcal{Q}}_{12}(e_1) & \bar{\mathcal{Q}}_{22}(e_1)\end{bmatrix}, \\ \bar{\mathcal{Q}}_{11}(e_1) &= 2(k_1p_{11} + k_2p_{12})\phi_1'(e_1),\ \bar{\mathcal{Q}}_{12}(e_1) = (k_1p_{12} + k_2p_{22} - p_{11})\phi_1'(e_1),\ \bar{\mathcal{Q}}_{22}(e_1) = -2p_{12}\phi_1'(e_1).\end{aligned} \tag{27}$$

With (27) and (19), we obtain $\bar{\mathcal{Q}} = \mathcal{Q}\mathcal{D}(e_1)$. Afterwards, with $\mathcal{Q}$, $\mathcal{D}(e_1) \succ 0$, as defined in (19) and (25), following inequality on their eigenvalues holds: With $\mathcal{Q} \succ 0$ and $\mathcal{D}(e_1) \succ 0$, we obtain following inequality on their eigenvalues,

$$\lambda_{\min}\left\{\mathcal{Q}\mathcal{D}(e_1)\right\} \geq \lambda_{\min}\left\{\mathcal{Q}\right\}\lambda_{\min}\left\{\mathcal{D}(e_1)\right\} > 0. \tag{28}$$

With Property 2, substituting (28) into (26) we obtain

$$\begin{aligned}\dot{V} &= -\zeta^{\mathrm{T}}(\mathcal{Q}\mathcal{D}(e_1))\zeta \\ &\leq -\lambda_{\min}\left\{\mathcal{Q}\mathcal{D}(e_1)\right\}\zeta^{\mathrm{T}}\zeta \\ &\leq -\lambda_{\min}\left\{\mathcal{D}(e_1)\right\}\lambda_{\min}\left\{\mathcal{Q}\right\}\zeta^{\mathrm{T}}\zeta\end{aligned} \tag{29}$$

With $\lambda_{\min}\left\{\mathcal{D}(e_1)\right\} = \lambda_{\min}\left\{\phi_1'(e_1)\right\}$, substituting (17) and (22) into (29), we obtain,

$$\begin{aligned}\dot{V} &\leq -\left[k_3 + (e_1^{\mathrm{T}}e_1)^{\frac{1-p}{3p-2}}\frac{p}{3p-2}\right]\lambda_{\min}\left\{\mathcal{Q}\right\}\zeta^{\mathrm{T}}\zeta \\ &\leq -\frac{\lambda_{\min}\left\{\mathcal{Q}\right\}}{\lambda_{\max}\left\{\mathcal{P}\right\}}\left[k_3 + \left(\frac{V}{\lambda_{\min}\left\{\mathcal{P}\right\}}\right)^{\frac{1-p}{p}}\frac{p}{3p-2}\right]V \\ &\leq -\gamma_1 V - \gamma_2 V^{\frac{1}{p}},\end{aligned} \tag{30}$$

where γ_1 and γ_2 are positive constants, defined as,

$$\gamma_1 = k_3\frac{\lambda_{\min}\left\{\mathcal{Q}\right\}}{\lambda_{\max}\left\{\mathcal{P}\right\}} = k_3\frac{\lambda_{\min}\left\{\mathcal{Q}^*\right\}}{\lambda_{\max}\left\{\mathcal{P}^*\right\}};\ \gamma_2 = \frac{\lambda_{\min}\left\{\mathcal{Q}\right\}\lambda_{\min}\left\{\mathcal{P}\right\}^{\frac{p-1}{p}}}{\lambda_{\max}\left\{\mathcal{P}\right\}}\frac{p}{3p-2} = \frac{\lambda_{\min}\left\{\mathcal{Q}^*\right\}\lambda_{\min}\left\{\mathcal{P}^*\right\}^{\frac{p-1}{p}}}{\lambda_{\max}\left\{\mathcal{P}^*\right\}}\frac{p}{3p-2}. \tag{31}$$

Therefore, based on the inequality (30), Lemma 1 and Lemma 2, we conclude that the origin of the error dynamics (12) is finite-time stable and fast finite-time stable. □

Corollary 1 (Disturbance Robustness)**.** Consider the proposed HC-FFTSD (12) in Theorem 1 under perturbation, $\delta = (\delta_1^{\mathrm{T}}, \delta_2^{\mathrm{T}})^{\mathrm{T}}$, $\delta_1, \delta_2 \in \mathbb{R}^n$, and δ is bounded as $||\delta|| \leq \bar{\delta}$. Thereafter, the differentiator under perturbation is as

$$\begin{aligned}\dot{e}_1 &= -k_1\phi_1(e_1) + e_2 + \delta_1, \\ \dot{e}_2 &= -k_2\phi_2(e_1) + \delta_2.\end{aligned} \tag{32}$$

When γ_1 in (31) fulfills $\gamma_1 \geq \lambda_{\max}\left\{\mathcal{P}\right\}/\lambda_{\min}\left\{\mathcal{P}\right\}$, (32) is Practically Finite-Time Stable (PFTS).

Proof. Consider the Lyapunov stability analysis in Theorem 1. With the Lyapunov-candidate defined by (20) and the expression of the differentiator under perturbation in (32), we express the time derivative of (20) as follows:

$$\dot{V} \leq -\gamma_1 V - \gamma_2 V^{\frac{1}{p}} + 2\lambda_{\max}\left\{\mathcal{P}\right\}\bar{\delta}||\zeta||. \tag{33}$$

By applying Cauchy-Schwarz inequality and (21), from (33), we obtain,

$$\begin{aligned}\dot{V} &\leq -\gamma_1 V - \gamma_2 V^{\frac{1}{p}} + \lambda_{\max}\left\{\mathcal{P}\right\}||\zeta||^2 + \lambda_{\max}\left\{\mathcal{P}\right\}\bar{\delta}^2 \\ &\leq -\left(\gamma_1 - \frac{\lambda_{\max}\left\{\mathcal{P}\right\}}{\lambda_{\min}\left\{\mathcal{P}\right\}}\right)V - \gamma_2 V^{\frac{1}{p}} + \lambda_{\max}\left\{\mathcal{P}\right\}\bar{\delta}^2.\end{aligned} \tag{34}$$

Therefore, according to Lemma 3, with inequality (34), we conclude that the system (32), which is the differentiator (12) under disturbance δ, is practical finite time stable at the origin.□

Corollary 2 (Noise Robustness)**.** Consider the proposed HC-FFTSD (12) in Theorem 1 under measurement noise μ, so that $\phi_1(e_1)$ and $\phi_2(e_1)$ in (10) are as $\phi_1(e_1+\mu)$ and $\phi_2(e_1+\mu)$. Thereafter

$$\begin{aligned}\dot{e}_1 &= -k_1\phi_1(e_1+\mu)+e_2\\ \dot{e}_2 &= -k_2\phi_2(e_1+\mu),\end{aligned} \tag{35}$$

where μ is bounded as $||\mu|| \le \bar{\mu}$. When γ_1 in (31) fulfills $\gamma_1 \ge \lambda_{\max}\{\mathcal{P}\}/\lambda_{\min}\{\mathcal{P}\}$, (35) is Practically Finite-Time Stable (PFTS).

Proof. From (35), we obtain the following expression

$$\begin{aligned}\dot{e}_1 &= -k_1\phi_1(e_1)+e_2+k_1\phi_1^*(e_1,\mu),\\ \dot{e}_2 &= -k_2\phi_2(e_1)+k_2\phi_2^*(e_1,\mu),\\ \phi_1^*(e_1,\mu) &= -\phi_1(e_1+\mu)+\phi_1(e_1),\\ \phi_2^*(e_1,\mu) &= -\phi_2(e_1+\mu)+\phi_2(e_1).\end{aligned} \tag{36}$$

With (10), we obtain

$$\begin{aligned}\phi_1^*(e_1,\mu) &= -\phi_1(e_1+\mu)+\phi_1(e_1)\\ &= -k_3\mu-\left[(e_1+\mu)^{\mathrm{T}}(e_1+\mu)\right]^{\frac{1-p}{3p-2}}(e_1+\mu)+(e_1^{\mathrm{T}}e_1)^{\frac{1-p}{3p-2}}e_1\\ \phi_2^*(e_1,\mu) &= -\phi_2(e_1+\mu)+\phi_2(e_1)\\ &= -k_3^2\mu-\frac{2k_3(2p-1)}{3p-2}\left[(e_1+\mu)^{\mathrm{T}}(e_1+\mu)\right]^{\frac{1-p}{3p-2}}(e_1+\mu)+\frac{2k_3(2p-1)}{3p-2}(e_1^{\mathrm{T}}e_1)^{\frac{1-p}{3p-2}}e_1\\ &\quad-\frac{p}{3p-2}\left[(e_1+\mu)^{\mathrm{T}}(e_1+\mu)\right]^{\frac{2(1-p)}{3p-2}}(e_1+\mu)+\frac{p}{3p-2}(e_1^{\mathrm{T}}e_1)^{\frac{2(1-p)}{3p-2}}e_1.\end{aligned}$$

Therefore, according to Lemma 5, we obtain the upper bounds of $\|\phi_1^*(e_1,\mu)\|$ and $\|\phi_2^*(e_1,\mu)\|$ as:

$$\begin{aligned}\|\phi_1^*(e_1,\mu)\| &\le k_3\bar{\mu}+2^{\frac{2(p-1)}{3p-2}}(\bar{\mu})^{1-\frac{2(p-1)}{3p-2}}\\ \|\phi_2^*(e_1,\mu)\| &\le k_3^2\bar{\mu}+\frac{2k_3(2p-1)}{3p-2}2^{\frac{2(p-1)}{3p-2}}(\bar{\mu})^{1-\frac{2(p-1)}{3p-2}}+\frac{p}{3p-2}2^{\frac{4(p-1)}{3p-2}}(\bar{\mu})^{1-\frac{4(p-1)}{3p-2}}\end{aligned}$$

Thus, with upper bounded $\|\phi_1^*(e_1,\mu)\|$ and $\|\phi_1^*(e_1,\mu)\|$, by Corollary 1, we conclude that the error dynamics (35) is PFTS at the origin.□

4 | PROBLEM FORMULATION

4.1 | Coordinate frame definition

The configuration of the UAV, modeled as a rigid body, is given by its position and orientation, which are together referred to as its pose. To define the pose of the vehicle, we fix a coordinate frame $\mathcal{B}$ to its body and another coordinate frame $\mathcal{I}$ that is fixed in space as the inertial coordinate frame. Define $\mathbf{e}_i$ as the unit vector along the axis of the three-dimension space. Let $b \in \mathbb{R}^3$ denote the position vector of the origin of frame $\mathcal{B}$ with respect to frame $\mathcal{I}$. Let SO(3) denote the orientation (attitude), defined as the rotation matrix from frame $\mathcal{B}$ to frame $\mathcal{I}$. The pose of the vehicle can be represented in matrix form as follows:

$$g = \begin{bmatrix} R & b\\ 0 & 1\end{bmatrix} \in \mathrm{SE(3)} \tag{37}$$

where SE(3), the special Euclidean group, is the six-dimensional Lie group of rigid body motions. A diagram of guidance and trajectory tracking on SE(3) through a set of waypoints is presented in Figure 1 as follows.

4.2 | System kinematics and dynamics

The instantaneous pose (position and attitude) is compactly represented by $\mathrm{g} = (b, R) \in \mathrm{SE(3)}$. The UAV's kinematics is then defined by:

$$\begin{cases}\dot{b} = v = Rv,\\ \dot{R} = R\Omega^{\times},\end{cases} \tag{38}$$

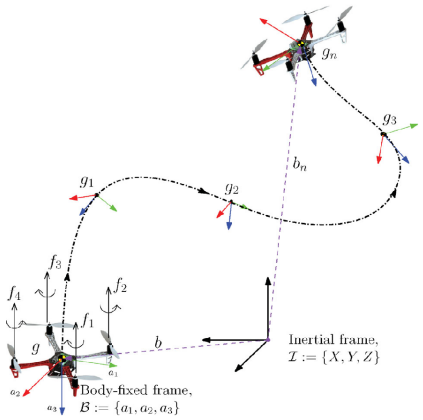

Figure 1 Guidance through a trajectory between initial and final configurations on SE(3)[40,27]

where $v \in \mathbb{R}^3$ and $\nu \in \mathbb{R}^3$ denote the translational velocity in frames $\mathcal{I}$ and $\mathcal{B}$ respectively, and $\Omega \in \mathbb{R}^3$ is the angular velocity in body-fixed frame $\mathcal{B}$. The overall system kinematics and dynamics of a rotorcraft UAV with a body-fixed plane of rotors are given by:

$$\begin{cases} \dot{b} = v = R\nu \\ m\dot{v} = mg\mathbf{e}_3 - fR\mathbf{e}_3 + \varphi_D \\ \dot{R} = R\Omega^{\times} \\ J\dot{\Omega} = J\Omega \times \Omega + \tau + \tau_D \end{cases} \tag{39}$$

where $\mathbf{e}_3 = [0 \quad 0 \quad 1]^{\mathrm{T}}$, $f \in \mathbb{R}$ is the scalar thrust force, and $\tau \in \mathbb{R}^3$ is the control torque created by the rotors, g denotes the acceleration due to gravity and $m \in \mathbb{R}^+$ and $J = J^{\mathrm{T}} \in \mathbb{R}^{3\times3}$ are the mass and inertia matrix of the UAV, respectively. The force and torque disturbances are denoted φ_D and τ_D respectively, which are mainly due to unsteady aerodynamics.

4.3 | Morse function on SO(3)

The following Lemma is utilized in the rotational ESO and attitude tracking control schemes for the aircraft.

Lemma 6. [41] Consider attitude kinematics

$$\dot{R} = R\Omega^{\times}, R \in \mathrm{SO}(3), \Omega \in \mathfrak{so}(3). \tag{40}$$

Define $K = \mathrm{diag}(K_1, K_2, K_3)$, where $K_1 > K_2 > K_3 \geq 1$. Define

$$s_K(R) = \sum_{i=1}^{3} K_i(R^{\mathrm{T}}\mathbf{e}_i) \times \mathbf{e}_i, \tag{41}$$

such that $\frac{\mathrm{d}}{\mathrm{d}t}\langle K, I - R\rangle = \Omega^{\mathrm{T}} s_K(R)$. Here $\langle A, B\rangle = \mathrm{tr}(A^{\mathrm{T}}B)$, which makes $\langle K, I - R\rangle$ a Morse function defined on SO(3). Let $\mathcal{S} \subset \mathrm{SO}(3)$ be a closed subset containing the identity in its interior, defined by

$$\mathcal{S} = \left\{R \in \mathrm{SO}(3) \ : \ R_{ii} \geq 0 \text{ and } R_{ij}R_{ji} \leq 0, \forall i, \ j \in \{1,2,3\}, \ i \neq j\right\}. \tag{42}$$

Then for $\forall R \in \mathcal{S}$, we have

$$s_K(R)^{\mathrm{T}} s_K(R) \geq \langle K, I - R\rangle. \tag{43}$$

Remark 1 (Almost global domain of attraction)**.** [42] We know that the subset of SO(3) where $s_K(R) = 0, R \in \mathrm{SO}(3)$, which is also the set of critical points for $\langle I - R, K\rangle$, is

$$C \triangleq \{I, \mathrm{diag}(1,-1,-1), \mathrm{diag}(-1,1,-1), \mathrm{diag}(-1,-1,1)\} \subset \mathrm{SO}(3). \tag{44}$$

In addition, the global minimum of Morse-Function is $R = I$.

4.4 | Tracking error kinematics and dynamics

Let $g^d(t) \in \mathrm{SE}(3)$ be the desired pose generated by a guidance scheme [27]. Let v^d and ν^d denote the desired translational velocity in the inertial frame $\mathcal{I}$ and the body frame $\mathcal{B}$, respectively, and Ω^d denote the body's reference angular velocity in the body frame. Then, the tracking error is given by,

$$\bar{h} = (\mathrm{g}^d)^{-1}\mathrm{g} = \begin{pmatrix} Q & x \\ 0 & 1 \end{pmatrix} \in \mathrm{SE}(3), \tag{45}$$

where $Q = (R^d)^{\mathrm{T}}R$ is the attitude tracking error, and $x = (R^d)^{\mathrm{T}}(b - b^d) = (R^d)^{\mathrm{T}}\tilde{b}$ is the position tracking error, both in the body-fixed frame. Also, the translation velocity tracking error is given by

$$\tilde{v} = v - v^d, \tag{46}$$

and the angular velocity tracking error is given by,

$$\omega = \Omega - Q^{\mathrm{T}}\Omega^d. \tag{47}$$

Thus, in the inertial frame $\mathcal{I}$, the translational tracking error kinematics and dynamics can be summarized as

$$\begin{aligned} \dot{\tilde{b}} &= \tilde{v}, \\ m\dot{\tilde{v}} &= mg\mathbf{e}_3 - fR\mathbf{e}_3 + \varphi_D - m\dot{v}^d. \end{aligned} \tag{48}$$

in the body-fixed frame $\mathcal{B}$, the attitude tracking error kinematics and dynamics can be summarized as

$$\begin{aligned} \dot{Q} &= Q\omega^{\times}, \\ J\dot{\omega} &= \tau + \tau_D + J(\omega^{\times}Q^{\mathrm{T}}\Omega^d - Q^{\mathrm{T}}\dot{\Omega}^d) - (J\Omega)\times(\omega + Q^{\mathrm{T}}\Omega^d). \end{aligned} \tag{49}$$

The rotational error dynamics is decoupled from the translational error dynamics such that the translation control force, f, is obtained in the inertial frame followed by the appropriate attitude tracking control law, τ, in body frame to track the desired trajectory, b^d.

4.5 | ESO estimations and errors

The ESO design on SE(3) is split into translational ESO design on vector space $\mathbb{R}^3$ and rotational ESO design on SO(3). Let $(\widehat{b}, \widehat{v}, \widehat{\varphi}_D) \in \mathbb{R}^3 \times \mathbb{R}^3 \times \mathbb{R}^3$ be the estimated translational position, velocity, and disturbance forces, as the states of translational ESO. The estimation errors of translational ESO are then defined as follows,

$$e_b = b - \widehat{b}, e_v = v - \widehat{v}, e_\varphi = \varphi_D - \widehat{\varphi}_D, \tag{50}$$

which are estimation errors of translational position, velocity, and total disturbance force respectively.

Let $(\widehat{R}, \widehat{\Omega}, \widehat{\tau}_D) \in \mathrm{SO}(3) \times \mathbb{R}^3 \times \mathbb{R}^3$ be the estimated attitude, angular velocity, and disturbance torque states provided by the rotational ESO. For the rotational ESO, the error states are defined as follows. Please note that the attitude estimation error can be defined as

$$E_R = \widehat{R}^{\mathrm{T}}R, \tag{51}$$

on the group of rigid body rotations, SO(3), which is not a vector space. The angular velocity estimation error, e_Ω, and torque disturbance estimation error, e_τ, are expressed on the vector space $\mathbb{R}^3$, and are defined as:

$$e_\Omega = \Omega - E_R^{\mathrm{T}}\widehat{\Omega},\ e_\tau = \tau_D - \widehat{\tau}_D. \tag{52}$$

With a proper ESO design on SE(3), the error states $(e_b, e_v, e\varphi)$ and (E_R, e_Ω, e_τ) will converge to $(0,0,0)$ and $(I,0,0)$, respectively. The ESO design and its stability proof will be described in detail in the following section.

5 | FAST FINITE-TIME STABLE EXTENDED STATE OBSERVER (FFTS-ESO) ON SE(3)

In this section, we present the FFTS-ESO on SE(3). As mentioned in the previous section, the ESO design on SE(3) can be represented as a translational ESO on the vector space $\mathbb{R}^3$ to estimate disturbance forces, and an rotational ESO on SO(3) to estimate disturbance torques. We present the ESO designs in two results and present their stability proofs in this section.

5.1 | ESO for Translational Motion

Proposition 1 (Translational ESO)**.** Consider the following ESO design for the translational motion:

$$\begin{aligned}
\dot{\hat{b}} &= \hat{v}, \\
m\dot{\hat{v}} &= mg\mathbf{e}_3 - fR\mathbf{e}_3 + mk_{t1}\phi_1(\psi_t) + m\kappa_t\left[(e_b^{\mathrm{T}}e_b)^{\frac{1-p}{p}} H\left(e_b, \frac{p-1}{p}\right)e_v + e_v\right] + \hat{\varphi}_D, \\
\dot{\hat{\varphi}}_D &= mk_{t2}\phi_2(\psi_t),
\end{aligned} \tag{53}$$

where ψ_t is defined as

$$\psi_t = e_v + \kappa_t\left[e_b + (e_b^{\mathrm{T}}e_b)^{\frac{1-p}{p}} e_b\right], \tag{54}$$

and $\phi_1(\cdot)$ is as defined in the expression in (10). In addition, we define the constant k_{t3}, which does not appear in the expressions (53) and (54), but occurs in the terms $\phi_1(\psi_t)$ and $\phi_2(\psi_t)$, where it takes the place of k_3 in (10). The positive scalar gains k_{t1}, k_{t2}, k_{t3}, and κ_t are constrained as follows.

- (Constraint 1) The matrix $\mathcal{A}_t \in \mathbb{R}^{2\times 2}$ defined as:

$$\mathcal{A}_t = \begin{bmatrix} -k_{t1} & 1 \\ -k_{t2} & 0 \end{bmatrix}, \tag{55}$$

  is a Hurwitz matrix.

- (Constraint 2) For $\mathcal{A}_t$ as defined above, $\forall\, \mathcal{Q}_t \in \mathbb{R}^{2\times 2}$ where $\mathcal{Q}_t \succ 0$, the Lyapunov equation,

$$\mathcal{A}_t^{\mathrm{T}}\mathcal{P}_t + \mathcal{P}_t\mathcal{A}_t = -\mathcal{Q}_t, \tag{56}$$

  has a unique solution $\mathcal{P}_t$. The eigenvalues of $\mathcal{Q}_t$ are constrained as follows:

$$k_{t3}\frac{\lambda_{\min}\{\mathcal{Q}_t\}}{\lambda_{\max}\{\mathcal{P}_t\}} - \frac{1}{k_{t3}^2\lambda_{\min}\{\mathcal{P}_t\}} > 0. \tag{57}$$

- (Constraint 3) $\kappa_t > 1/2$.

Theorem 2. With the observer errors for the translational ESO defined by (50), the translational kinematics and dynamics given by (39), and the ESO for translational motion given in Proposition 1, the error dynamics of the ESO is given by:

$$\begin{aligned}
\dot{e}_b &= e_v, \\
m\dot{e}_v &= -mk_{t1}\phi_1(\psi_t) - m\kappa_t\left[(e_b^{\mathrm{T}}e_b)^{\frac{1-p}{p}} H\left(e_b, \frac{p-1}{p}\right)e_v + e_v\right] + e_\varphi, \\
\dot{e}_\varphi &= -mk_{t2}\phi_2(\psi_t) + \dot{\varphi}_D.
\end{aligned} \tag{58}$$

The error dynamics (58) is FFTS at the origin ($(e_b, e_v, e_\varphi) = (0,0,0)$), when the resultant disturbance force is constant ($\dot{\varphi}_D = 0$), and the gains of the ESO are constrained according to Proposition 1.

Proof. Simplify (58) as:

$$\begin{aligned}
\dot{\psi}_t &= -k_{t1}\phi_1(\psi_t) + m^{-1}e_\varphi, \\
m^{-1}\dot{e}_\varphi &= -k_{t2}\phi_2(\psi_t) + m^{-1}\dot{\varphi}_D.
\end{aligned} \tag{59}$$

Next, define the Lyapunov function to prove Theorem 2:

$$V_t = V_{t0} + e_b^{\mathrm{T}}e_b, \text{ where } V_{t0} = \zeta_t^{\mathrm{T}}\mathcal{P}_t\zeta_t \tag{60}$$

and ζ_t is defined as:

$$\zeta_t = [\phi_1^{\mathrm{T}}(\psi_t),\ m^{-1}e_\varphi^{\mathrm{T}}]^{\mathrm{T}}.$$

From Theorem 1, (59) and (23), we find that the time-derivative of V_t satisfies:

$$\dot{V}_t \leq -\gamma_{t1}V_{t0} - \gamma_{t2}V_{t0}^{\frac{1}{p}} + 2e_b^{\mathrm{T}}e_v, \tag{61}$$

where γ_{t1} and γ_{t2} are defined by:

$$\gamma_{t1} = k_{t3}\frac{\lambda_{\min}\left\{\mathcal{Q}_t\right\}}{\lambda_{\max}\left\{\mathcal{P}_t\right\}}, \quad \gamma_{t2} = \frac{\lambda_{\min}\left\{\mathcal{Q}_t\right\}\lambda_{\min}\left\{\mathcal{P}_t\right\}^{\frac{p-1}{p}}p}{\lambda_{\max}\left\{\mathcal{P}_t\right\}(3p-2)}. \tag{62}$$

Substituting (54) into (61), we obtain:

$$\begin{aligned}
\dot{V}_t &\leq -\gamma_{t1}V_{t0} - \gamma_{t2}V_{t0}^{\frac{1}{p}} + 2e_b^{\mathrm{T}}\left[\psi_t - \kappa_t e_b - \kappa_t(e_b^{\mathrm{T}}e_b)^{\frac{1-p}{p}}e_b\right] \\
&\leq -\gamma_{t1}V_{t0} - \gamma_{t2}V_{t0}^{\frac{1}{p}} + 2e_b^{\mathrm{T}}\psi_t - 2\kappa_t e_b^{\mathrm{T}}e_b - 2\kappa_t(e_b^{\mathrm{T}}e_b)^{\frac{1}{p}} \\
&\leq -\gamma_{t1}V_{t0} - \gamma_{t2}V_{t0}^{\frac{1}{p}} - 2\kappa_t e_b^{\mathrm{T}}e_b - 2\kappa_t(e_b^{\mathrm{T}}e_b)^{\frac{1}{p}} + \psi_t^{\mathrm{T}}\psi_t + e_b^{\mathrm{T}}e_b \\
&\leq -\left(\gamma_{t1} - \frac{1}{k_{t3}^2\lambda_{\min}\left\{\mathcal{P}_t\right\}}\right)V_{t0} - \gamma_{t2}V_{t0}^{\frac{1}{p}} - (2\kappa_t - 1)e_b^{\mathrm{T}}e_b - 2\kappa_t(e_b^{\mathrm{T}}e_b)^{\frac{1}{p}}.
\end{aligned} \tag{63}$$

Therefore, we further obtain:

$$\dot{V}_t < -\Gamma_{t1}V_t - \Gamma_{t2}V_t^{\frac{1}{p}}, \tag{64}$$

where

$$\Gamma_{t1} = \min\left\{k_{t3}\frac{\lambda_{\min}\left\{\mathcal{Q}_t\right\}}{\lambda_{\max}\left\{\mathcal{P}_t\right\}} - \frac{1}{k_{t3}^2\lambda_{\min}\left\{\mathcal{P}_t\right\}}, 2\kappa_t - 1\right\},\ \Gamma_{t2} = \min\left\{\frac{\lambda_{\min}\left\{\mathcal{Q}_t\right\}\lambda_{\min}\left\{\mathcal{P}_t\right\}^{\frac{p-1}{p}}p}{\lambda_{\max}\left\{\mathcal{P}_t\right\}(3p-2)}, 2\kappa_t\right\}. \tag{65}$$

Based on (64), we conclude that when the resultant disturbance force is constant, and the ESO gains satisfy the constraints 1-3 in Proposition 1, the error dynamics of the ESO (58) is FFTS. This concludes the proof of Theorem 2. □

5.2 | ESO for Rotational Motion

Proposition 2 (Rotational ESO)**.** Define $e_R = s_k(E_R)$, where $s_K(\cdot)$ is as defined by Lemma 6. Define $e_w(E_R, e_\Omega)$ as follows:

$$e_w(E_R, e_\Omega) = \frac{\mathrm{d}}{\mathrm{d}t}e_R = \sum_{i=1}^{3} K_i\mathbf{e}_i \times (e_\Omega \times E_R^{\mathrm{T}}\mathbf{e}_i). \tag{66}$$

Consider the following ESO design:

$$\begin{aligned}
&\dot{\widehat{R}} = \widehat{R}\widehat{\Omega}^{\times}, \\
&\dot{\widehat{\Omega}} = E_R J^{-1}\left[J\Omega\times\Omega + \widehat{\tau}_D + \tau + k_{a1}J\phi_1(\psi_a) + \kappa_a J(e_R^{\mathrm{T}}e_R)^{\frac{1-p}{p}}H\left(e_R, \frac{p-1}{p}\right)e_w + \kappa_a J e_w\right] + E_R e_\Omega^{\times}E_R^{\mathrm{T}}\widehat{\Omega}, \\
&\dot{\widehat{\tau}}_D = J k_{a2}\phi_2(\psi_a),
\end{aligned} \tag{67}$$

where ψ_a is defined as follows:

$$\psi_a = e_\Omega + \kappa_a\left[e_R + (e_R^{\mathrm{T}}e_R)^{\frac{1-p}{p}}e_R\right]. \tag{68}$$

In addition, we define the constant k_{a3}, which occurs in the terms $\phi_1(\psi_a)$ and $\phi_2(\psi_a)$, where it takes the place of k_3 in (10). The positive scalar gains k_{a1}, k_{a2}, k_{a3}, and κ_a are constrained as follows.

- (Constraint 1) The matrix $\mathcal{A}_a \in \mathbb{R}^{2\times2}$ defined as:

$$\mathcal{A}_a = \begin{bmatrix} -k_{a1} & 1 \\ -k_{a2} & 0 \end{bmatrix}, \tag{69}$$

is a Hurwitz matrix.

- (Constraint 2) For $\mathcal{A}_a$ as defined above and $\forall\, \mathcal{Q}_a \in \mathbb{R}^{2\times 2}$ where $\mathcal{Q}_a \succ 0$, the Lyapunov equation:

$$\mathcal{A}_a^{\mathrm{T}}\mathcal{P}_a + \mathcal{P}_a\mathcal{A}_a = -\mathcal{Q}_a, \tag{70}$$

has a unique solution $\mathcal{P}_a$. The eigenvalues of $\mathcal{Q}_a$ and $\mathcal{P}_a$ are constrained as follows:

$$k_{a3}\frac{\lambda_{\min}\left\{\mathcal{Q}_a\right\}}{\lambda_{\max}\left\{\mathcal{P}_a\right\}} - \frac{1}{2k_{a3}^2\lambda_{\min}\left\{\mathcal{P}_a\right\}} > 0. \tag{71}$$

- (Constraint 3) $\kappa_a > 1/2$.

Theorem 3. With the observer errors for the rotational ESO defined by (52), the rotational kinematics and dynamics given by (39), and the ESO for rotational motion given in Proposition 2, the error dynamics of the ESO is given by:

$$\begin{aligned}
\dot{E}_R &= E_R e_\Omega^{\times},\\
J\dot{e}_\Omega &= -k_{a1}J\phi_1(\psi_a) - \kappa_a J\left[(e_R^{\mathrm{T}}e_R)^{\frac{1-p}{p}}H\left(e_R, \frac{p-1}{p}\right)e_w + e_w\right] + e_\tau,\\
\dot{e}_\tau &= -k_{a2}J\phi_2(\psi_a) + \dot{\tau}_D.
\end{aligned} \tag{72}$$

The error dynamics (58) is almost globally FFTS (AG-FFTS) at the origin ($(E_R, e_\Omega, e_\tau) = (I, 0, 0)$), when the resultant disturbance torque is constant ($\dot{\tau}_D = 0$), and the gains of the ESO are constrained according to Proposition 2.

Proof. Simplify (72) as:

$$\begin{aligned}
\dot{\psi}_a &= -k_{a1}\phi_1(\psi_a) + J^{-1}e_\tau,\\
J^{-1}\dot{e}_\tau &= -k_{a2}\phi_2(\psi_a) + J^{-1}\dot{\tau}_D.
\end{aligned} \tag{73}$$

Next, define the Morse-Lyapunov function to prove Theorem 3:

$$V_a = V_{a0} + \langle K, I - E_R\rangle, \text{ where } V_{a0} = \zeta_a^{\mathrm{T}}\mathcal{P}_a\zeta_a \tag{74}$$

and ζ_a is defined as:

$$\zeta_a = [\phi_1^{\mathrm{T}}(\psi_a),\ J^{-1}e_\tau^{\mathrm{T}}]^{\mathrm{T}}.$$

From Theorem 1, (73) and (23), we find that the time-derivative of V_a satisfies:

$$\dot{V}_a \le -\gamma_{a1}V_{a0} - \gamma_{a2}V_{a0}^{\frac{1}{p}} + e_R^{\mathrm{T}}e_\Omega, \tag{75}$$

where γ_{a1} and γ_{a2} are defined by:

$$\gamma_{a1} = k_{a3}\frac{\lambda_{\min}\left\{\mathcal{Q}_a\right\}}{\lambda_{\max}\left\{\mathcal{P}_a\right\}}, \quad \gamma_{a2} = \frac{\lambda_{\min}\left\{\mathcal{Q}_a\right\}\lambda_{\min}\left\{\mathcal{P}_a\right\}^{\frac{p-1}{p}}p}{\lambda_{\max}\left\{\mathcal{P}_a\right\}(3p-2)}. \tag{76}$$

Substituting (68) into (75), we obtain,

$$\begin{aligned}
\dot{V}_a &\le -\gamma_{a1}V_{a0} - \gamma_{a2}V_{a0}^{\frac{1}{p}} + e_R^{\mathrm{T}}\left[\psi_a - \kappa_a e_R - \kappa_a(e_R^{\mathrm{T}}e_R)^{\frac{1-p}{p}}e_R\right]\\
&\le -\gamma_{a1}V_{a0} - \gamma_{a2}V_{a0}^{\frac{1}{p}} + e_R^{\mathrm{T}}\psi_a - \kappa_a e_R^{\mathrm{T}}e_R - \kappa_a(e_R^{\mathrm{T}}e_R)^{\frac{1}{p}}\\
&\le -\gamma_{a1}V_{a0} - \gamma_{a2}V_{a0}^{\frac{1}{p}} - \kappa_a e_R^{\mathrm{T}}e_R - \kappa_a(e_R^{\mathrm{T}}e_R)^{\frac{1}{p}} + \frac{1}{2}\psi_a^{\mathrm{T}}\psi_a + \frac{1}{2}e_R^{\mathrm{T}}e_R\\
&\le -\left(\gamma_{a1} - \frac{1}{2k_{a3}^2\lambda_{\min}\left\{\mathcal{P}_a\right\}}\right)V_{a0} - \gamma_{a2}V_{a0}^{\frac{1}{p}} - \left(\kappa_a - \frac{1}{2}\right)e_R^{\mathrm{T}}e_R - \kappa_a(e_R^{\mathrm{T}}e_R)^{\frac{1}{p}}
\end{aligned} \tag{77}$$

By applying Lemma 6 on (75), we obtain,

$$\dot{V}_a \le -\left(\gamma_{a1} - \frac{1}{2k_{a3}^2\lambda_{\min}\left\{\mathcal{P}_a\right\}}\right)V_{a0} - \gamma_{a2}V_{a0}^{\frac{1}{p}} - \left(\kappa_a - \frac{1}{2}\right)\langle K, I - E_R\rangle - \kappa_a\langle K, I - E_R\rangle^{\frac{1}{p}} \tag{78}$$

Therefore, we further obtain:

$$\dot{V}_a \le -\Gamma_{a1}V_a - \Gamma_{a2}V_a^{\frac{1}{p}}, \tag{79}$$

where,

$$\Gamma_{a1} = \min\left\{ k_{a3}\frac{\lambda_{\min}\left\{\mathcal{Q}_a\right\}}{\lambda_{\max}\left\{\mathcal{P}_a\right\}} - \frac{1}{2k_{a3}^2\lambda_{\min}\left\{\mathcal{P}_a\right\}}, \kappa_a - \frac{1}{2} \right\},\ \Gamma_{a2} = \min\left\{ \frac{\lambda_{\min}\left\{\mathcal{Q}_a\right\}\lambda_{\min}\left\{\mathcal{P}_a\right\}^{\frac{p-1}{p}}\, p}{\lambda_{\max}\left\{\mathcal{P}_a\right\}(3p-2)}, \kappa_a \right\}. \tag{80}$$

Consider the expression given by (79), the set where $\dot{V}_a = 0$ is:

$$\dot{V}_a^{-1}(0) = \left\{(E_R, e_\Omega, e_\tau) : s_K(E_R) = 0, \text{and } \zeta_a = 0\right\} = \left\{(E_R, e_\Omega, e_\tau) : E_R \in C, e_\Omega = 0, \text{and } e_\tau = 0\right\}, \tag{81}$$

where C is defined by (44), which express the set of the critical points. With Theorem 8.4 from Khalil[43], we conclude that (E_R, e_Ω, e_τ) converge to the set:

$$S = \left\{(E_R, e_\Omega, e_\tau) \in \mathrm{SO}(3)\times\mathbb{R}^3\times\mathbb{R}^3 : E_R \in C, e_\Omega = 0, \text{and } e_\tau = 0\right\}, \tag{82}$$

in finite time.

Based on (79), and Lemma 2, we conclude that when the ESO gains satisfy the constraints in Proposition 2, the set of equilibrium S for the error dynamics (72) is fast finite time stable.

In S, the only stable equilibrium is $(I, 0, 0)$, while the other three are unstable. The resulting closed-loop system with the estimation errors gives rise to a Hölder-continuous feedback with exponent less than one ($1/2 < 1/p < 1$), while in the limiting case of $p = 1$, the feedback system is Lipschitz-continuous. Proceeding with a topological equivalence-based analysis similar to the one by Bohn et al.[41], we conclude that the equilibrium and the corresponding regions of attraction of the rotational ESO with $p \in]1, 2[$ are identical to those of the corresponding Lipschitz-continuous asymptotically stable ESO with $p = 1$, and the region of attraction is almost global.

To summarize, we conclude that the error dynamics (58) is almost globally FFTS (AG-FFTS) at the origin ($(E_R, e_\Omega, e_\tau) = (I, 0, 0)$), when the resultant disturbance torque is constant ($\dot{\tau}_D = 0$), and the gains of the ESO are constrained according to Proposition 2. This concludes the proof of Theorem 3. □

Remark 2 (Disturbance robustness of the ESO)**.** Consider Corollary 1 and its constraints on differentiator gains. When the disturbance forces and torques are time-varying, then $\|\dot{\varphi}_D\|, \|\dot{\tau}_D\| > 0$. Further, if the constraints on gains in Corollary 1 are fulfilled, the estimation error dynamics of the proposed ESO will be practically finite-time stable (PFTS).

Remark 3 (Noise robustness of the ESO)**.** Consider Corollary 2 and its constraints on differentiator gains. When the ESO measurements have noise and the constraints on gains in Corollary 2 are fulfilled, the estimation error dynamics of the proposed ESO will be PFTS. Moreover, according to Lemma 3 and Corollary 2, the η in (6) of Lemma 3 is a function on the level of noise in information on R, Ω, b and v and is monotonically increasing with the level of noise.

Remark 4 (Comparative Analysis of Noise Robustness: FFTS-ESO vs. the FxTSDO by Liu et al.[12])**.** We investigate the disturbance (forces or torques) observers proposed by Liu et al.[12] in their Theorems 1 and 2, known as FxTSDO. The input of FxTSDO relies on the motion signals, X_2, Y_2, which represent translational and angular velocities, and $\dot{X}_2$, $\dot{Y}_2$, which represent translational and angular accelerations, respectively.

However, the high-level noise associated with the translational acceleration obtained from an accelerometer, restricts its direct use in a flight control scheme. Additionally, direct measurement of angular acceleration is usually not feasible.

Furthermore, if $\dot{X}_2$ and $\dot{Y}_2$ are obtained from finite difference of X_2 and Y_2, they will have higher noise levels than X_2 and Y_2, leading to inferior disturbance estimation performance.

In contrast to FxTSDO, the proposed FFTS-ESO incorporates position and attitude signals, which are zero-order derivatives of motions with lower noise level. Consequently, FFTS-ESO outperforms FxTSDO in terms of disturbance estimation performance, despite the theoretical fixed-time stability of FxTSDO. We show this through our numerical simulations in Section 7.

6 | FAST-FINITE TIME STABLE ACTIVE DISTURBANCE REJECTION CONTROL (FFTS-ADRC) ON SE(3)

A robust ADRC on SE(3) is presented in this section and it is split into position and attitude tracking modules. The proposed FFTS-ESO on SE(3) presented in Section 5 is utilized here to provide disturbance estimates $\widehat{\varphi}_D$ and $\widehat{\tau}_D$. For tracking control, e_φ and e_τ are not only disturbance estimation errors in (58) and (72), but they are also the disturbance rejection errors. The

stability proof of the proposed ADRC includes both tracking error dynamics in (48)-(49) and ESO estimation error dynamics in (58) and (72). This stability proof does not treat the disturbance estimation/rejection errors e_φ and e_τ as zero vectors, but as error terms updated according to propositions 1 and (2). This means that the disturbance estimation errors in the proposed ESO are designed to converge much faster than the tracking errors in ADRC. With our Lyapunov stability analysis, we analyze the coupling between the tracking control and ESO schemes, and how that influences gain tuning for ADRC scheme.

6.1 | ADRC for Translational Motion Control

Proposition 3 (Position Tracking ADRC)**.** Given the tracking error kinematics and dynamics in (48), consider the translational motion tracking control law:

$$\varphi = f R\mathbf{e}_3 = mg\mathbf{e}_3 + k_{TD}L_T\left[\psi_T + (\psi_T^{\mathrm{T}}\psi_T)^{\frac{1-p}{p}}\psi_T\right] + k_{TP}L_T\tilde{b} + m\kappa_T\left[\tilde{v} + (\tilde{b}^{\mathrm{T}}\tilde{b})^{\frac{1-p}{p}}H\left(\tilde{b}, \frac{p-1}{p}\right)\tilde{v}\right] - m\dot{v}_d + \widehat{\varphi}_D, \tag{83}$$

where ψ_T is defined as:

$$\psi_T = \tilde{v} + \kappa_T\left[\tilde{b} + (\tilde{b}^{\mathrm{T}}\tilde{b})^{\frac{1-p}{p}}\tilde{b}\right], \tag{84}$$

and $\widehat{\varphi}_D$ is obtained from the translational ESO in Proposition 1. In addition to the ESO gains defined in Proposition 1, define positive scalar control gains κ_T, k_{TD}, k_{TP}, and a positive definite diagonal matrix $L_T = \mathrm{diag}(L_{T1}, L_{T2}, L_{T3})$ that satisfy the following constraints:

- (Constraint 1) k_{TD} and L_T are constrained as:

$$k_{TD}\lambda_{\min}\{L_T\} - \frac{1}{2} > 0.$$

- (Constraint 2) The decay constant for the translational ESO Γ_{t1} defined by (65), $\mathcal{P}_t$ given by (56), and the rotorcraft mass m are constrained as:

$$\Gamma_{t1} - \frac{m^2}{2\lambda_{\min}\{\mathcal{P}_t\}} > 0.$$

Theorem 4. With the translational tracking errors defined by (45), kinematics and dynamics given by (48), ESO error dynamics given by (58), and the ADRC for position tracking given in Proposition 3, the translational tracking error dynamics satisfies:

$$\begin{aligned}\dot{\tilde{b}} &= \tilde{v}\\ m\dot{\tilde{v}} &= e_\varphi - k_{TD}L_T\left[\psi_T + (\psi_T^{\mathrm{T}}\psi_T)^{\frac{1-p}{p}}\psi_T\right] - k_{TP}L_T\tilde{b} - m\kappa_T\left[\tilde{v} + (\tilde{b}^{\mathrm{T}}\tilde{b})^{\frac{1-p}{p}}H\left(\tilde{b}, \frac{p-1}{p}\right)\tilde{v}\right],\end{aligned} \tag{85}$$

where e_φ is updated by the translational ESO error dynamics according to (58). The tracking error dynamics (85) combined with the ESO error dynamics (58) is FFTS at the origin ($(\tilde{b}, \tilde{v}, e_b, e_v, e_\varphi) = (0, 0, 0, 0, 0)$), when the resultant disturbance force is constant ($\dot{\varphi}_D = 0$), and the gains of the ESO and ADRC schemes are constrained according to Proposition 1 and Proposition 3.

Proof. Simplify (85) as:

$$\begin{aligned}\dot{\tilde{b}} &= \tilde{v}\\ m\dot{\psi}_T &= e_\varphi - k_{TD}L_T\left[\psi_T + (\psi_T^{\mathrm{T}}\psi_T)^{\frac{1-p}{p}}\psi_T\right] - k_{TP}L_T\tilde{b}.\end{aligned} \tag{86}$$

Next, define the Lyapunov function:

$$V_T = V_t + \frac{1}{2}m\psi_T^{\mathrm{T}}\psi_T + \frac{1}{2}k_{TP}\tilde{b}^{\mathrm{T}}\tilde{b}, \tag{87}$$

where V_t is defined by (60) in the proof of Theorem 2. We obtain the time-derivative of this Lyapunov function (87) as:

$$\begin{aligned}
\dot{V}_T &= m\psi_T^{\mathrm{T}}\dot{\psi}_T + k_{TP}\tilde{b}^{\mathrm{T}}\dot{\tilde{b}} + \dot{V}_t \\
&\leq \psi_T^{\mathrm{T}} e_\varphi - k_{TD}\psi_T^{\mathrm{T}} L_T \psi_T - k_{TD}(\psi_T^{\mathrm{T}}\psi_T)^{\frac{1-p}{p}}\psi_T^{\mathrm{T}} L_T \psi_T - k_{TP}\psi_T^{\mathrm{T}}\tilde{b} + k_{TP}\tilde{b}^{\mathrm{T}}\tilde{v} - \Gamma_{t1}V_t - \Gamma_{t2}V_t^{\frac{1}{p}} \\
&\leq \frac{1}{2}\psi_T^{\mathrm{T}}\psi_T + \frac{1}{2}e_\varphi^{\mathrm{T}} e_\varphi - k_{TD}\lambda_{\min}\{L_T\}\psi_T^{\mathrm{T}}\psi_T - k_{TD}\lambda_{\min}\{L_T\}(\psi_T^{\mathrm{T}}\psi_T)^{\frac{1}{p}} \\
&- k_{TP}\psi_T^{\mathrm{T}}\tilde{b} + k_{TP}\tilde{b}^{\mathrm{T}}\Big[\psi_T - \kappa_T(\tilde{b} + (\tilde{b}^{\mathrm{T}}\tilde{b})^{\frac{1-p}{p}}\tilde{b})\Big] - \Gamma_{t1}V_t - \Gamma_{t2}V_t^{\frac{1}{p}} \\
&\leq -\Big(k_{TD}\lambda_{\min}\{L_T\} - \frac{1}{2}\Big)\psi_T^{\mathrm{T}}\psi_T - k_{TD}\lambda_{\min}\{L_T\}(\psi_T^{\mathrm{T}}\psi_T)^{\frac{1}{p}} \\
&- \kappa_T k_{TP}(\tilde{b}^{\mathrm{T}}\tilde{b}) - \kappa_T k_{TP}(\tilde{b}^{\mathrm{T}}\tilde{b})^{\frac{1}{p}} - \Big(\Gamma_{t1} - \frac{m^2}{2\lambda_{\min}\{\mathcal{P}_t\}}\Big)V_t - \Gamma_{t2}V_t^{\frac{1}{p}} \\
&\leq -\left(2k_{TD}\lambda_{\min}\{L_T\} - 1\right)m^{-1}\Big(\frac{1}{2}m\psi_T^{\mathrm{T}}\psi_T\Big) - 2^{\frac{1}{p}}k_{TD}\lambda_{\min}\{L_T\}m^{-\frac{1}{p}}\left(\frac{1}{2}m\psi_T^{\mathrm{T}}\psi_T\right)^{\frac{1}{p}} \\
&- 2\kappa_T\Big(\frac{1}{2}k_{TP}\tilde{b}^{\mathrm{T}}\tilde{b}\Big) - 2^{\frac{1}{p}}\kappa_T k_{TP}^{\frac{p-1}{p}}\Big(\frac{1}{2}k_{TP}\tilde{b}^{\mathrm{T}}\tilde{b}\Big)^{\frac{1}{p}} - \Big(\Gamma_{t1} - \frac{m^2}{2\lambda_{\min}\{\mathcal{P}_t\}}\Big)V_t - \Gamma_{t2}V_t^{\frac{1}{p}},
\end{aligned} \tag{88}$$

where Γ_{t1}, Γ_{t2} and $\mathcal{P}_t$ are as defined in the proof of Theorem 2. Thus, we obtain the following inequality:

$$\dot{V}_T \leq -\Gamma_{T1}V_T - \Gamma_{T2}V_T^{\frac{1}{p}}, \tag{89}$$

where Γ_{T1} and Γ_{T2} are defined by:

$$\Gamma_{T1} = \min\left\{\left(2k_{TD}\lambda_{\min}\{L_T\} - 1\right)m^{-1}, 2\kappa_T, \Gamma_{t1} - \frac{m^2}{2\lambda_{\min}\{\mathcal{P}_t\}}\right\}, \Gamma_{T2} = \min\left\{2^{\frac{1}{p}}k_{TD}\lambda_{\min}\{L_T\}m^{-\frac{1}{p}}, 2^{\frac{1}{p}}\kappa_T k_{TP}^{\frac{p-1}{p}}, \Gamma_{t2}\right\}. \tag{90}$$

Based on (89), we conclude that when the resultant disturbance force is constant ($\dot{\varphi}_D = 0$), and the ESO and ADRC gains satisfy the constraints in Proposition 1 and Proposition 3, the tracking error dynamics (85) for the translational motion is FFTS. This concludes the proof of Theorem 4. □

With this translational motion control scheme, a desired control force vector $\varphi = fR\mathbf{e}_3 \in \mathbb{R}^3$ is generated. With $fR\mathbf{e}_3$ obtained in this manner, the methodology utilized in §3.3 of[27] can be employed to generate the desired (reference) attitude profile to be tracked by the attitude control system, which is described in the following subsection. The term r_{3d} in[27], which denotes the third column of the rotation matrix, is re-defined here as $r_{3d} := \varphi/||\varphi||$. The rest of the tracking control design is similar to what has already been used in our prior research[27,40].

6.2 | ADRC for Rotational Motion Control

Proposition 4 (Attitude Tracking ADRC)**.** Given the tracking error kinematics and dynamics in (49), consider the attitude tracking control law

$$\begin{aligned}
\tau = &-k_{AD}L_A\Big[\psi_A + (\psi_A^{\mathrm{T}}\psi_A)^{\frac{1-p}{p}}\psi_A\Big] - k_{AP}s_K(Q) - k_{AI}\psi_{AI} - J(Q^{\mathrm{T}}\dot{\Omega}^d - \omega^{\times}Q^{\mathrm{T}}\Omega^d) - J\Omega\times\Omega - \widehat{\tau}_D \\
&- \kappa_A J\Big[w(Q,\omega) + (s_K(Q)^{\mathrm{T}}s_K(Q))^{\frac{1-p}{p}}H\Big(s_K(Q), \frac{p-1}{p}\Big)w(Q,\omega)\Big], \\
\dot{\psi}_{AI} = &-L_A\psi_{AI} - L_A(\psi_{AI}^{\mathrm{T}}\psi_{AI})^{\frac{1-p}{p}}\psi_{AI} + \psi_A
\end{aligned} \tag{91}$$

where ψ_{AI} is defined as an integral term initialized with $\psi_{AI}(0) = 0$, ψ_A is defined as:

$$\psi_A = \omega + \kappa_A\Big[s_K(Q) + (s_K(Q)^{\mathrm{T}}s_K(Q))^{\frac{1-p}{p}}s_K(Q)\Big], \tag{92}$$

$s_K(Q)$ is defined by Lemma 6, $w(Q,\omega)$ is defined as

$$w(Q,\omega) = \frac{\mathrm{d}}{\mathrm{d}t}s_K(Q) = \sum_{i=1}^{3} K_i\mathbf{e}_i \times (\omega \times Q^{\mathrm{T}}\mathbf{e}_i), \tag{93}$$

and $\widehat{\tau}_D$ is obtained from the rotational ESO in Proposition 2. In addition to the ESO gains defined in Proposition 2, define positive scalar gains κ_A, k_{AD}, k_{AP}, k_{AI}, and a positive definite diagonal matrix gain $L_A = \mathrm{diag}(L_{A1}, L_{A2}, L_{A3})$ that satisfy the following constraints:

- (Constraint 1) k_{AD} and L_A are constrained as

$$2k_{AD}\lambda_{\min}\{L_A\} - 1 > 0.$$

- (Constraint 2) The decay constant for the rotational ESO Γ_{a1} defined by (80), $\mathcal{P}_a$ given by (70), and the rotorcraft inertia J are constrained as:

$$\Gamma_{a1} - \frac{1}{2}\lambda_{\min}\{J^{-2}\}^{-1}\lambda_{\min}\{\mathcal{P}_a\}^{-1} > 0.$$

Theorem 5. With the attitude tracking errors defined by (45), kinematics and dynamics given by (49), ESO error dynamics given by (72), and the ADRC for attitude tracking given in Proposition 4, the rotational tracking error dynamics of the ADRC is given by:

$$\begin{aligned}
\dot{Q} &= Q\omega \\
J\dot{\omega} &= e_\tau - k_{AD}L_A\Big[\psi_A + (\psi_A^{\mathrm{T}}\psi_A)^{\frac{1-p}{p}}\psi_A\Big] - k_{AP}s_K(Q) - k_{AI}\psi_{AI} \\
&\quad - \kappa_A\Big[w(Q,\omega) + (s_K(Q)^{\mathrm{T}}s_K(Q))^{\frac{1-p}{p}}H\Big(s_K(Q), \frac{p-1}{p}\Big)w(Q,\omega)\Big] \\
\dot{\psi}_{AI} &= -L_A\psi_{AI} - L_A(\psi_{AI}^{\mathrm{T}}\psi_{AI})^{\frac{1-p}{p}}\psi_{AI} + \psi_A,
\end{aligned} \tag{94}$$

where e_τ is updated by the rotational ESO error dynamics given by (72). The tracking error dynamics given by (94), combined with the ESO error dynamics given by (72), is almost globally fast finite-time stable (AG-FFTS) at $((Q,\omega,\psi_{AI},E_R,e_\Omega,e_\tau) = (I,0,0,I,0,0))$, when the resultant disturbance torque is constant ($\dot{\tau}_D = 0$), and the gains of the ESO and ADRC schemes are constrained according to Proposition 2 and Proposition 4.

Proof. Simplify (94) as:

$$\begin{aligned}
\dot{Q} &= Q\omega \\
J\dot{\psi}_A &= e_\tau - k_{AD}L_A\Big[\psi_A + (\psi_A^{\mathrm{T}}\psi_A)^{\frac{1-p}{p}}\psi_A\Big] - k_{AP}s_K(Q) - k_{AI}\psi_{AI} \\
\dot{\psi}_{AI} &= -L_A\psi_{AI} - L_A(\psi_{AI}^{\mathrm{T}}\psi_{AI})^{\frac{1-p}{p}}\psi_{AI} + \psi_A.
\end{aligned} \tag{95}$$

Next, define the following Morse-Lyapunov function:

$$V_A = V_a + \frac{1}{2}\psi_A^{\mathrm{T}}J\psi_A + k_{AP}\langle K, I-Q\rangle + \frac{1}{2}k_{AI}\psi_{AI}^{\mathrm{T}}\psi_{AI}, \tag{96}$$

where V_a is defined by (74) in the proof of Theorem 3. We obtain the time derivative of V_A as:

$$\begin{aligned}
\dot{V}_A &= \dot{V}_a + \psi_A^{\mathrm{T}}J\dot{\psi}_A + k_{AP}s_K(Q)^{\mathrm{T}}\omega + k_{AI}\psi_{AI}^{\mathrm{T}}\dot{\psi}_{AI} \\
&\le -\Gamma_{a1}V_a - \Gamma_{a2}V_a^{\frac{1}{p}} + \psi_A^{\mathrm{T}}e_\tau - k_{AD}\psi_A^{\mathrm{T}}L_A\Big[\psi_A + (\psi_A^{\mathrm{T}}\psi_A)^{\frac{1-p}{p}}\psi_A\Big] - k_{AP}\psi_A^{\mathrm{T}}s_K(Q) - k_{AI}\psi_A^{\mathrm{T}}\psi_{AI} + k_{AP}\psi_A^{\mathrm{T}}s_K(Q) \\
&\quad - k_{AP}\kappa_A s_K(Q)^{\mathrm{T}}\Big[s_K(Q) + (s_K(Q)^{\mathrm{T}}s_K(Q))^{\frac{1-p}{p}}s_K(Q)\Big] - k_{AI}\psi_{AI}^{\mathrm{T}}L_A\psi_{AI} - k_{AI}(\psi_{AI}^{\mathrm{T}}\psi_{AI})^{\frac{1-p}{p}}\psi_{AI}^{\mathrm{T}}L_A\psi_{AI} + k_{AI}\psi_{AI}^{\mathrm{T}}\psi_A \\
&\le -\Gam_{a1}V_a - \Gamma_{a2}V_a^{\frac{1}{p}} + \frac{1}{2}e_\tau^{\mathrm{T}}e_\tau - \Big(k_{AD}\lambda_{\min}\{L_A\} - \frac{1}{2}\Big)\psi_A^{\mathrm{T}}\psi_A - k_{AD}\lambda_{\min}\{L_A\}(\psi_A^{\mathrm{T}}\psi_A)^{\frac{1}{p}} \\
&\quad - k_{AP}\kappa_A s_K(Q)^{\mathrm{T}}s_K(Q) - k_{AP}\kappa_A(s_K(Q)^{\mathrm{T}}s_K(Q))^{\frac{1}{p}} - k_{AI}\lambda_{\min}\{L_A\}\psi_{AI}^{\mathrm{T}}\psi_{AI} - k_{AI}\lambda_{\min}\{L_A\}(\psi_{AI}^{\mathrm{T}}\psi_{AI})^{\frac{1}{p}} \\
&\le -\Big[\Gamma_{a1} - \big(2\lambda_{\min}\{J^{-2}\}\lambda_{\min}\{\mathcal{P}_a\}\big)^{-1}\Big]V_a - \Gamma_{a2}V_a^{\frac{1}{p}} - \kappa_A k_{AP}\langle K, I-Q\rangle - \kappa_A k_{AP}^{\frac{p-1}{p}}(k_{AP}\langle K, I-Q\rangle)^{\frac{1}{p}} \\
&\quad - \Big(2k_{AD}\lambda_{\min}\{L_A\} - 1\Big)\lambda_{\max}\{J\}^{-1}\Big(\frac{1}{2}\psi_A^{\mathrm{T}}J\psi_A\Big) - 2^{\frac{1}{p}}k_{AD}\lambda_{\min}\{L_A\}\lambda_{\max}\{J\}^{-\frac{1}{p}}\Big(\frac{1}{2}\psi_A^{\mathrm{T}}J\psi_A\Big)^{\frac{1}{p}} \\
&\quad - 2\lambda_{\min}\{L_A\}\Big(\frac{1}{2}k_{AI}\psi_{AI}^{\mathrm{T}}\psi_{AI}\Big) - 2^{\frac{1}{p}}k_{AP}^{\frac{p-1}{p}}\lambda_{\min}\{L_A\}\Big(\frac{1}{2}k_{AI}\psi_{AI}^{\mathrm{T}}\psi_{AI}\Big)^{\frac{1}{p}},
\end{aligned} \tag{97}$$

where Γ_{a1}, Γ_{a2} and $\mathcal{P}_a$ are defined by 76 in the proof of Theorem 3. Simplify (97):

$$\dot{V}_A \le -\Gamma_{A1}V_A - \Gamma_{A2}V_A^{\frac{1}{p}} \tag{98}$$

where Γ_{A1} and Γ_{A2} are defined as:

$$\Gamma_{A1} = \min\left\{\left(\Gamma_{a1} - \frac{1}{2}\lambda_{\min}\{J^{-2}\}^{-1}\lambda_{\min}\{\mathcal{P}_a\}^{-1}\right),\ 2\left(k_{AD}\lambda_{\min}\{L_A\} - \frac{1}{2}\right)\lambda_{\max}\{J\}^{-1},\ \kappa_A,\ 2\lambda_{\min}\{L_A\}\right\},$$
$$\Gamma_{A2} = \min\left\{\Gamma_{a2},\ 2^{\frac{1}{p}}k_{AD}\lambda_{\min}\{L_A\}\lambda_{\max}\{J\}^{-\frac{1}{p}},\ \kappa_A k_{AP}^{\frac{p-1}{p}},\ 2^{\frac{1}{p}}k_{AP}^{\frac{p-1}{p}}\lambda_{\min}\{L_A\}\right\}.$$

Based on (98), we conclude that when the resultant disturbance torque is constant ($\dot{\tau}_D = 0$), and the ESO and ADRC gains satisfy the constraints in Proposition 2 and Proposition 4, the tracking error dynamics (94) is AG-FFTS. Since the discussion on the equilibrium set including SO(3) is covered in the proof of Theorem 3, we omit it here in this proof for brevity. This concludes the proof of Theorem 5. □

7 | NUMERICAL SIMULATIONS

In this section, we present several sets of numerical simulations, arranged in two subsections to validate the proposed ESO and ADRC. In subsection 7.1, we compare the proposed FFTS-ESO with the existing ESO[11] and DO[12] designs, on their disturbance estimation performance in different flight scenarios. Subsection 7.2 describes the numerical simulation of the ADRC proposed in Section 6 in different flight scenarios with the controlled dynamics numerically simulated by a geometric integrator[33].

7.1 | The comparison between FFTS-ESO and other ESO/DO design

We compare the proposed FFTS-ESO with existing disturbance estimation schemes, which are LESO[11] and FxTSDO[12], on their disturbance estimation performance in four different simulated flight scenarios, with and without the presence of measurement noises. The four flight scenarios correspond to four desired trajectories. The inertia and mass of the simulated rotorcraft UAV are $J = \text{diag}([0.0820, 0.0845, 0.1377])\ \text{kg}\cdot\text{m}^2$, $m = 4.34\ \text{kg}$[44]. Since the target of the simulation is to validate and compare the disturbance estimation performance, the actuator dynamics and saturation are not included in the results reported in this section. The tracking control scheme to drive the UAV to track the desired trajectories is the tracking control scheme reported in Section 6 without disturbance rejection terms, such that $\widehat{\tau}_D = 0$ in (91) and $\widehat{\varphi}_D = 0$ in (83). We use the MATLAB/Simulink software with ODE4 (Runge-Kutta fourth order) solver to conduct this set of simulations. The time step size is $h = 0.001$s and the simulated duration is $T = 25$s.

Hovering	$b_d(t) = [0,\ 0,\ -3]^{\mathrm{T}}$ (m)
Slow Swing	$b_d(t) = [10\sin(0.1\pi t),\ 0,\ -3]^{\mathrm{T}}$ (m)
Fast Swing	$b_d(t) = [5\sin(0.5\pi t),\ 0,\ -3]^{\mathrm{T}}$ (m)
High Pitch	$b_d(t) = [10\sin(0.5\pi t),\ 10\cos(0.5\pi t),\ -3]^{\mathrm{T}}$ (m)

Table 1 Flight trajectories to be tracked for the comparisons between LESO, FxTSDO and FFTS-ESO

b_{N}	$b_{\mathrm{N}} = b + \mu_b$	$\mu_b \sim P_b = 3e-8$
v_{N}	$v_{\mathrm{N}} = v + \mu_v$	$\mu_v \sim P_v = 3e-7$
R_{N}	$R_{\mathrm{N}} = R\exp(\mu_R)$	$\mu_R \sim P_R = 3e-8$
Ω_{N}	$\Omega_{\mathrm{N}} = \Omega + \mu_\Omega$	$\mu_\Omega \sim P_\Omega = 3e-7$

Table 2 Measurement noise level in power spectral density for the comparisons between LESO, FxTSDO and FFTS-ESO

The four flight scenarios are the four desired trajectories listed in Table 1. 'Hovering' is the simplest flight scenario where the aircraft is ordered to hover at a fixed position during the simulation. 'High Pitch' is the most complex flight scenario where the

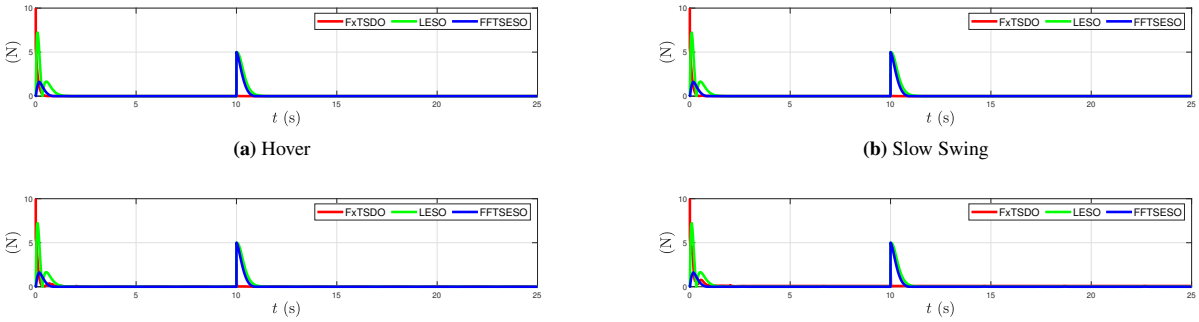

(a) Hover **(b)** Slow Swing

(c) Fast Swing **(d)** High Pitch

Figure 2 Disturbance force estimation errors of the multi-rotor UAV from FxTSDO, LESO, and the proposed FFTS-ESO, in four different tracking control scenarios without measurement noise.

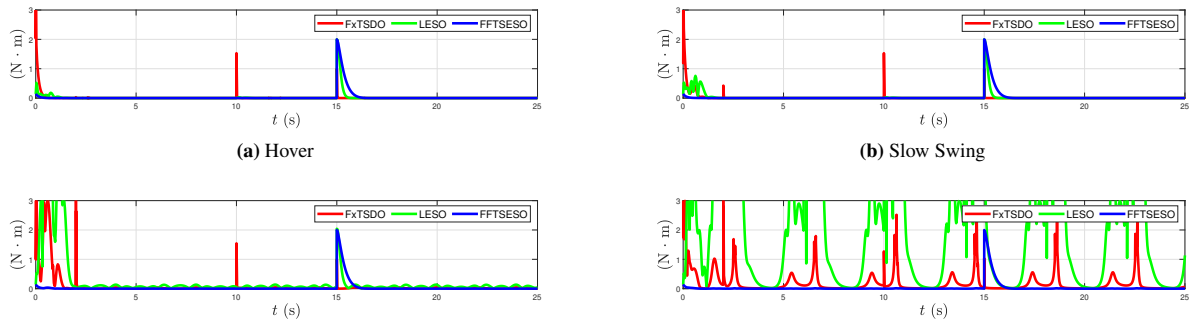

(a) Hover **(b)** Slow Swing

(c) Fast Swing **(d)** High Pitch

Figure 3 Disturbance torque estimation errors of the multi-rotor UAV from FxTSDO, LESO, and the proposed FFTS-ESO, in four different tracking control scenarios without measurement noise.

aircraft has to pitch up and track a circular trajectory. Since the norm of centripetal acceleration in 'High Pitch' scenario is more than a g, the aircraft has to flip over to track the desired trajectory. This desired trajectory with high centripetal acceleration forces the aircraft to go past the 90° pitch singularity of an Euler angle attitude representation. The measurement noise levels are as listed in Table 2 in terms of power spectral density (PSD). In this set of numerical simulations, the trajectory is tracked by the tracking control system placed in Section 6 without the disturbance rejection term $\hat{\varphi}_D$ and $\hat{\tau}_D$. The disturbance force and torque in all of the four scenarios in this set of simulations are identical and they are the following step functions:

$$\varphi_D(t) = \begin{cases} [5,\ 2,\ 0]^{\mathrm{T}}\ \mathrm{N} & t < 10\ \mathrm{s} \\ [9,\ 5,\ 0]^{\mathrm{T}}\ \mathrm{N} & t \geq 10\ \mathrm{s} \end{cases},\ \tau_D(t) = \begin{cases} [2,\ 0,\ 1]^{\mathrm{T}}\ \mathrm{N \cdot m} & t < 15\ \mathrm{s} \\ [4,\ 0,\ 1]^{\mathrm{T}}\ \mathrm{N \cdot m} & t \geq 15\ \mathrm{s} \end{cases}$$

The parameters for FFTS-ESO in these simulations are $p = 1.2, k_{t1} = 3, k_{t2} = 2, k_{t3} = 2, \kappa_t = 0.1, k_{a1} = 5, k_{a2} = 4, k_{a3} = 2, \kappa_a = 0.3$. The parameters for the tracking control scheme in the simulations are $p = 1.2, k_{TP} = 5, k_{TD} = 16, L_P = I, \kappa_T = 2, k_{AP} = 12, k_{AD} = 6, k_{AI} = 2, \kappa_A = 2, L_A = I$. The gains for FxTSDO and LESO are as given in Liu et al.[12] and Shao et al.[11]. In the simulated flight, the initial states of the UAV for all four scenarios are:

$$R(0) = I,\ \Omega(0) = [0,\ 0,\ 0]^{\mathrm{T}}\ \mathrm{rad/s}, b(0) = [0.01,\ 0,\ 0]^{\mathrm{T}}\ \mathrm{m},\ v(0) = [5\pi,\ 0,\ 0]^{\mathrm{T}}\ \mathrm{m/s}.$$

The initial conditions of the FxTSDO, LESO and FFTS-ESO, are identical to the pose, velocities and disturbance of the UAV at the initial time in the simulation.

We present the simulation results in four sets of figures. Figures 2 and 3 present the disturbance force and torque estimation errors respectively, from FxTSDO, LESO and FFTS-ESO in the flight scenarios described in Table 1 with noise-free measurements. Figures 4 and 5 present the disturbance estimation errors from these schemes for the flight trajectories in Table 1, in the presence of measurement noise levels as described in Table 2.

Figure 2 shows the disturbance force estimation errors from the three schemes with noise-free measurements. Although the disturbance force estimation error from FxTSDO shows significant initial transient, the results from Figure 2 indicates that with noise-free measurement, the disturbance force estimations from these three schemes converge to the origin in all four flight scenarios. The transients at $t = 15$ s are from the step-function disturbance force φ_D, whose step time is $t = 15$ s. Figure 3 shows the disturbance torque estimation errors from the three schemes with noise-free measurement. In Figure 3, we observe that when $t = 10$ s, high transients appears in the disturbance torque estimation error from FxTSDO.

Despite the initial transients, the disturbance torque estimation errors from all three schemes converge to the origin in 'Hovering' and 'Slow swing' scenarios. However, in 'Fast swing' and 'High pitch' scenarios, the disturbance torque estimation errors from LESO and FxTSDO diverge. As is stated in Section 1, since the LESO uses Euler-angle to represent attitude for disturbance torque estimation, it experiences a singularity in attitude representation when the UAV tracks the 'Fast swing' and 'High Pitch' trajectories. Thus, in these two scenarios, the singularity in the attitude representation destabilizes the disturbance torque estimation error of LESO.

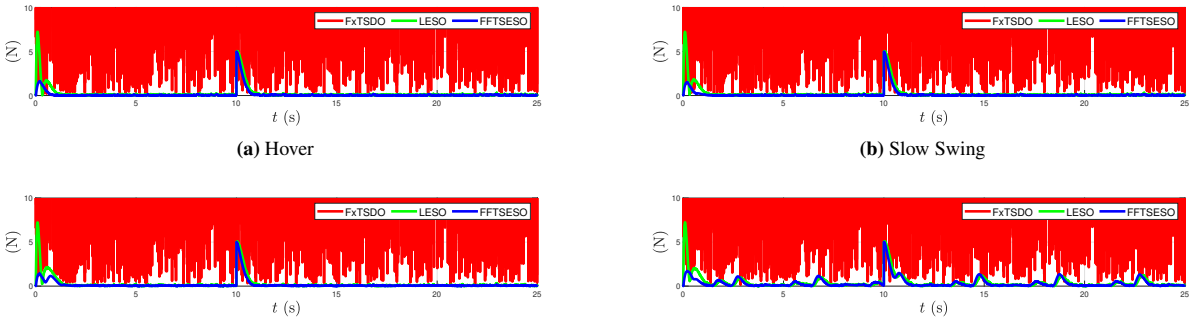

(a) Hover **(b)** Slow Swing

(c) Fast Swing **(d)** High Pitch

Figure 4 Disturbance force estimation errors of the multi-rotor UAV from FxTSDO, LESO, and the proposed FFTS-ESO, in four different tracking control scenarios with measurement noise.

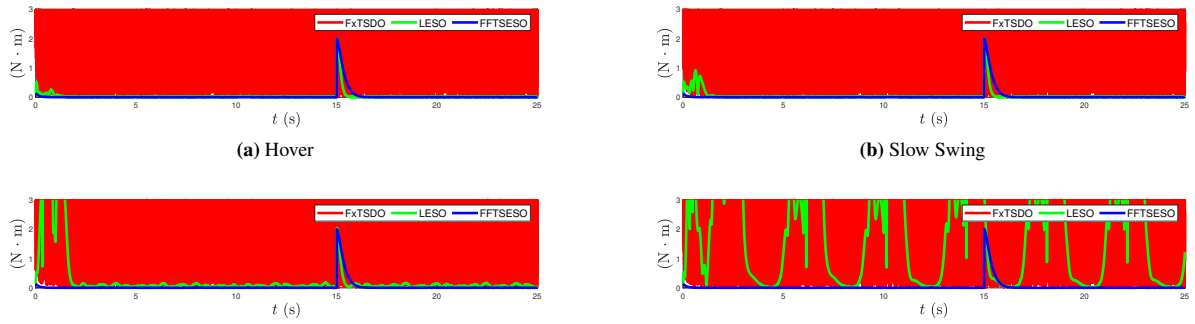

(a) Hover **(b)** Slow Swing

(c) Fast Swing **(d)** High Pitch

Figure 5 Disturbance torque estimation errors of the multi-rotor UAV from FxTSDO, LESO, and the proposed FFTS-ESO, in four different tracking control scenarios with measurement noise.

Figures 4 and 5 present the disturbance force and disturbance torque estimation errors respectively, from the three schemes with identical noisy measurements as given in Table 2. As is stated in Remark 4, we observe that with measurement noise, FxTSDO is not capable of providing any meaningful disturbance estimation. In 'Fast swing' and 'High pitch' scenarios, the disturbance torque estimation errors from LESO diverge from the origin.

To summarize, figures 2, 3, 4, and 5 show that the FFTS-ESO has satisfactory disturbance estimation performance and outperforms the LESO and FxTSDO when the UAV experiences large pose changes and has noisy measurements.

7.2 | Simplified simulation with LGVI

In this subsection, we present a set of numerical simulation results on the FFTS-ADRC scheme, based on the geometric integrator LGVI[33]. The inertia and mass of the aircraft is $J = \text{diag}([0.0820, 0.0845, 0.1377])\ \text{kg}\cdot\text{m}^2$, $m = 4.34$ kg. The motion of the UAV is numerically integrated in discrete time with a LGVI[33]. The simulated time duration is $T = 5$s, with a time step size of $\Delta t = 0.005$s. The ESO and control gains of the implemented FFTS-ADRC are: $k_{t1} = 5; k_{t2} = 5; k_{t3} = 3; \kappa_t = 2; k_{TD} = 4;\ L_T = I; k_{TP} = 2; \kappa_T = 2, k_{a1} = 5; k_{a2} = 6; k_{a3} = 3; \kappa_a = 1.5; k_{AD} = 3;\ L_A = 0.5I; k_{AP} = 3; k_{AI} = 0.1; \kappa_A = 2; p = 1.2$. The desired trajectory of the simulation is given by:

$$b_d(t) = [2\sin(\pi t),\ 2t,\ 2\sin(\pi t)]^{\mathrm{T}}\ \text{m},$$

resulting in the aircraft experiencing a singularity in the Euler angle attitude representation.

The dynamic disturbance force and torque in all of the four scenarios in this set of simulations are identical and they are the following functions:

$$\varphi_D(t) = \left[50 + 6\sin\left(\frac{\pi t}{2}\right) + \frac{1}{2}\sin(\pi t),\ 50 + 3\sin\left(\frac{\pi t}{2}\right) + \frac{1}{5}\sin(\pi t),\ 20\right]^{\mathrm{T}}\ \text{N}$$
$$\tau_D(t) = \left[5 + \frac{1}{2}\sin\left(\frac{\pi t}{2}\right) + \frac{1}{10}\sin(\pi t),\ 3 + \sin\left(\frac{\pi t}{2}\right) + \frac{1}{20}\sin(\pi t),\ -3\right]^{\mathrm{T}}\ \text{N}\cdot\text{m}$$

In the simulated flight, the initial states of the UAV for all four scenarios are:

$$R(0) = I,\ \Omega(0) = [0,\ 0,\ 0]^{\mathrm{T}}\ \text{rad/s}, b(0) = [0,\ 0,\ 3]^{\mathrm{T}}\ \text{m},\ v(0) = [2\pi,\ 0,\ 0]^{\mathrm{T}}\ \text{m/s}.$$

The initial conditions of the FFTS-ESO are identical to the pose, velocities and disturbance inputs of the UAV at the initial time for this simulation.

Four sets of simulation results, namely simulation without disturbance rejection, with only disturbance force rejection, with only disturbance torque rejection, and with both disturbance force and disturbance torque rejection, are included in this section to validate the control performance of the proposed FFTS-ADRC scheme. The results are presented in Figure 6 and Figure 7. From Figure 6, we observe that all of the trajectories of the simulated flights converge to a neighborhood near the desired trajectory. Among these trajectories of the simulated flights, the one with both disturbance force and disturbance torque rejection is the one closest to the desired trajectory.

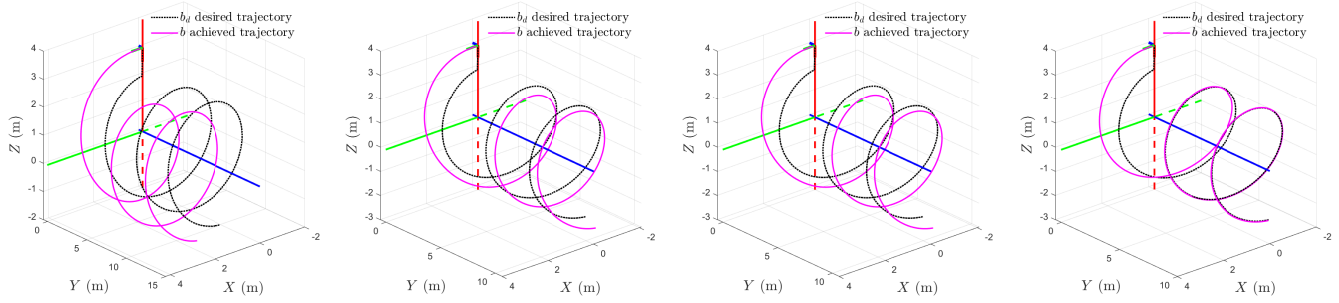

(a) Without rejection **(b)** Disturbance force rejection **(c)** Disturbance torque rejection **(d)** With both rejection

Figure 6 The tracked trajectories of the proposed FFTS-ADRC with different configurations of disturbance rejection

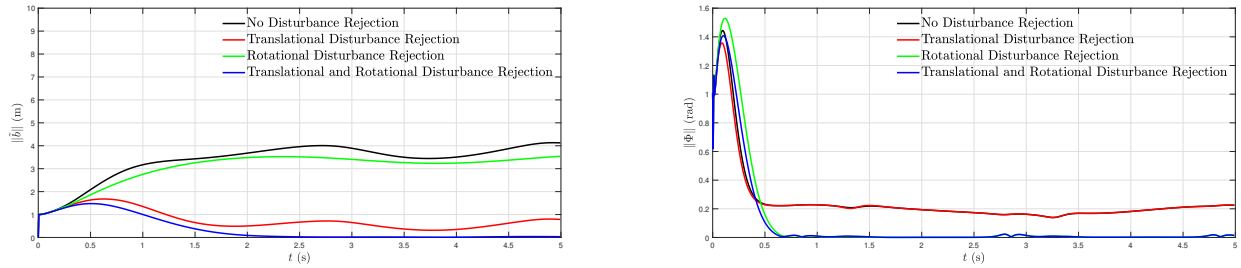

(a) Position tracking error

(b) Attitude tracking error

Figure 7 Position and attitude tracking error of the proposed FFTS-ADRC with different configurations of disturbance rejection

Figure 7 shows the results for the attitude and position tracking errors. The attitude tracking error is parameterized by the principal rotation angle Φ of the attitude tracking error matrix Q as,

$$\Phi = \cos^{-1}\left(\frac{1}{2}(\mathrm{tr}(Q) - 1)\right).$$

The position tracking error is defined as the norm of $\tilde{b}$. To clarify, in Figure 7, the $\|\Phi\|$ curve of the simulated flight without disturbance rejection and the one with only disturbance force rejection are almost identical to each other. Figure 7 indicates that the simulated flight with both disturbance force and disturbance torque rejection has the best control performance.

8 | CONCLUSION

In this article, a feedback tracking geometric control scheme using a FFTS-ESO for disturbance rejection is designed for rotorcraft UAV that have a body-fixed thrust direction and three-axis attitude control. The resulting FFTS-ADRC scheme enables such rotorcraft UAV to perform large maneuvers in the presence of aerodynamic uncertainties. The UAV is modeled as an underactuated system on the tangent bundle of the six-dimensional Lie group of rigid body motions, SE(3). The proposed ESO scheme is developed based on the HC-FFTSD, which is similar to the STA used in sliding mode designs, to obtain fast finite-time stability with higher tunability of the settling time compared to other FTS schemes. The ADRC scheme on SE(3), which utilizes the estimated disturbances from the ESO, is then incorporated to achieve FFTS tracking errors under constant disturbances and ultimate boundedness of tracking errors for time-varying disturbances. The Lyapunov stability analysis presented in this article for both ESO scheme and tracking control scheme proves the finite-time stability and robustness of the overall ADRC on SE(3). Two sets of numerical simulations are conducted. The first set of numerical simulation results present the stable performance of the FFTS-ESO scheme in estimating external force and torque disturbances acting on the UAV in different scenarios. The behavior of the FFTS-ESO is compared with two state-of-the-art observers for disturbance estimation. Using a realistic set of data for several simulated flight scenarios of a rotorcraft UAV, numerical simulations show that the FFTS-ESO, unlike the LESO and FxTSDO, is always stable and its convergence is robust to measurement noise and pose singularities. The proposed FFTS-ADRC scheme is numerically implemented by a geometric integrator for a rotorcraft UAV model and numerical simulations are carried out to validate the developed FFTS-ESO and FFTS-ADRC schemes. The numerical results also demonstrate the stable performance of the FFTS-ADRC when the UAV carries out large maneuvers that lead to kinematic singularities in Euler angle attitude representation.

□

APPENDIX

A PROOF OF LEMMA 5

Proof. Represent x as a linear combination of μ and ν:

$$x = c_1\mu + c_2\nu, \tag{A1}$$

where ν is a vector perpendicular to μ, such that $\mu^{\mathrm{T}}\nu = 0$. Next, define two non-zero scalars, c_1, c_2. Using (A1), express Y in Lemma 5 in coordinates (c_1, c_2):

$$Y = \frac{c_1\mu + c_2\nu}{\left(c_1^2\|\mu\|^2 + c_2^2\|\nu\|^2\right)^{\alpha}} - \frac{(1+c_1)\mu + c_2\nu}{\left[(1+c_1)^2\|\mu\|^2 + c_2^2\|\nu\|^2\right]^{\alpha}}. \tag{A2}$$

Thereafter, we obtain its partial derivatives with respect to these coordinates:

$$\begin{aligned}
\frac{\partial Y}{\partial c_1} &= \frac{\mu}{\left(c_1^2\|\mu\|^2 + c_2^2\|\nu\|^2\right)^{\alpha}} - \frac{2\alpha c_1\|\mu\|^2(c_1\mu + c_2\nu)}{\left(c_1^2\|\mu\|^2 + c_2^2\|\nu\|^2\right)^{\alpha+1}} - \frac{\mu}{\left[(1+c_1)^2\|\mu\|^2 + c_2^2\|\nu\|^2\right]^{\alpha}} + \frac{2\alpha(1+c_1)\|\mu\|^2\left[(1+c_1)\mu + c_2\nu\right]}{\left[(1+c_1)^2\|\mu\|^2 + c_2^2\|\nu\|^2\right]^{\alpha+1}}, \\
\frac{\partial Y}{\partial c_2} &= \frac{\nu}{\left(c_1^2\|\mu\|^2 + c_2^2\|\nu\|^2\right)^{\alpha}} - \frac{2\alpha c_2\|\nu\|^2(c_1\mu + c_2\nu)}{\left(c_1^2\|\mu\|^2 + c_2^2\|\nu\|^2\right)^{\alpha+1}} - \frac{\nu}{\left[(1+c_1)^2\|\mu\|^2 + c_2^2\|\nu\|^2\right]^{\alpha}} + \frac{2\alpha c_2\|\nu\|^2\left[(1+c_1)\mu + c_2\nu\right]}{\left[(1+c_1)^2\|\mu\|^2 + c_2^2\|\nu\|^2\right]^{\alpha+1}}.
\end{aligned} \tag{A3}$$

Thereafter, we employ the fact that the local maxima of $Y^{\mathrm{T}}Y$ satisfy:

$$\frac{\partial}{\partial c_1}(Y^{\mathrm{T}}Y) = \frac{\partial}{\partial c_2}(Y^{\mathrm{T}}Y) = 0,$$

we obtain the following equivalent conditions for the maxima:

$$\nu^{\mathrm{T}}\frac{\partial Y}{\partial c_1} = \mu^{\mathrm{T}}\frac{\partial Y}{\partial c_2} = 0, \tag{A4}$$

$$\mu^{\mathrm{T}}\frac{\partial Y}{\partial c_1} = 0, \tag{A5}$$

$$\nu^{\mathrm{T}}\frac{\partial Y}{\partial c_2} = 0. \tag{A6}$$

Substituting (A3) into (A4), we obtain:

$$\begin{aligned}
&\nu^{\mathrm{T}}\frac{\partial Y}{\partial c_1} = \mu^{\mathrm{T}}\frac{\partial Y}{\partial c_2} = 0, \Longleftrightarrow -\frac{2\alpha c_1 c_2\|\mu\|^2\|\nu\|^2}{\left(c_1^2\|\mu\|^2 + c_2^2\|\nu\|^2\right)^{\alpha+1}} + \frac{2\alpha(1+c_1)c_2\|\mu\|^2\|\nu\|^2}{\left[(1+c_1)^2\|\mu\|^2 + c_2^2\|\nu\|^2\right]^{\alpha+1}} = 0, \\
&\Rightarrow c_1\left[(1+c_1)^2\|\mu\|^2 + c_2^2\|\nu\|^2\right]^{\alpha+1} = (1+c_1)\left[c_1^2\|\mu\|^2 + c_2^2\|\nu\|^2\right]^{\alpha+1}, \qquad \text{(A7)} \\
&\text{or } c_2 = 0. \qquad \text{(A8)}
\end{aligned}$$

Substituting (A3) into (A5), we obtain:

$$\begin{aligned}
&\mu^{\mathrm{T}}\frac{\partial Y}{\partial c_1} = 0, \Rightarrow \frac{(1 - 2\alpha\|\mu\|^2c_1^2)\|\mu\|^2}{\left(c_1^2\|\mu\|^2 + c_2^2\|\nu\|^2\right)^{\alpha+1}} - \frac{\left[1 - 2\alpha(1+c_1)^2\|\mu\|^2\right]\|\mu\|^2}{\left[(1+c_1)^2\|\mu\|^2 + c_2^2\|\nu\|^2\right]^{\alpha+1}} = 0, \\
&\Longleftrightarrow (1+c_1)^2 = c_1^2, \Longleftrightarrow c_1 = -\frac{1}{2}.
\end{aligned} \tag{A9}$$

Substituting (A3) into (A6), we obtain:

$$\begin{aligned}
&\nu^{\mathrm{T}}\frac{\partial Y}{\partial c_2} = 0, \Rightarrow \frac{(1 - 2\alpha\|\nu\|^2c_2^2)\|\nu\|^2}{\left(c_1^2\|\mu\|^2 + c_2^2\|\nu\|^2\right)^{\alpha+1}} - \frac{(1 - 2\alpha\|\nu\|^2c_2^2)\|\nu\|^2}{\left[(1+c_1)^2\|\mu\|^2 + c_2^2\|\nu\|^2\right]^{\alpha+1}} = 0, \\
&\Longleftrightarrow (1+c_1)^2 = c_1^2, \Longleftrightarrow c_1 = -\frac{1}{2}.
\end{aligned} \tag{A10}$$

(A7) does not give a real solution for $\alpha \in]0, 1/2[$. Thus, we conclude that the only solution to (A4), (A5), (A6) is given by $c_1 = -1/2, c_2 = 0$. Thus, the only critical value of $Y^{\mathrm{T}}Y$ is obtained when $x = -\mu/2$. Further, we conclude that the global maximum of $Y^{\mathrm{T}}Y$ is at $x = -\mu/2$ because it is positive definite in Y. Therefore, we do not need an analysis of the Hessian matrix of $Y^{\mathrm{T}}Y$ as a function of (c_1, c_2). □

References

1. Torrente G, Kaufmann E, Föhn P, Scaramuzza D. Data-driven MPC for quadrotors. *IEEE Robotics and Automation Letters* 2021; 6(2): 3769–3776.
2. Hanover D, Foehn P, Sun S, Kaufmann E, Scaramuzza D. Performance, precision, and payloads: Adaptive nonlinear mpc for quadrotors. *IEEE Robotics and Automation Letters* 2021; 7(2): 690–697.
3. Bangura M, Mahony R. Thrust control for multirotor aerial vehicles. *IEEE Transactions on Robotics* 2017; 33(2): 390–405.
4. Craig W, Yeo D, Paley DA. Geometric Attitude and Position Control of a Quadrotor in Wind. *Journal of Guidance, Control, and Dynamics* 2020: 1–14.
5. Bisheban M, Lee T. Geometric adaptive control with neural networks for a quadrotor in wind fields. *IEEE Transactions on Control Systems Technology* 2020; 29(4): 1533–1548.
6. Lee T, Leok M, McClamroch NH. Geometric tracking control of a quadrotor UAV on SE (3). In: 49th IEEE conference on decision and control (CDC). ; 2010: 5420–5425.
7. Hartlieb RJ. The cancellation of random disturbances in automatic control systems. *PhDT* 1956.
8. Huang Y, Xu K, Han J, Lam J. Flight control design using extended state observer and non-smooth feedback. In: . 1. Proceedings of the 40th IEEE Conference on Decision and Control (Cat. No. 01CH37228). ; 2001: 223–228.
9. Chen WH. Nonlinear disturbance observer-enhanced dynamic inversion control of missiles. *Journal of Guidance, Control, and Dynamics* 2003; 26(1): 161–166.
10. Basile G, Marro G. On the observability of linear, time-invariant systems with unknown inputs. *Journal of Optimization theory and applications* 1969; 3: 410–415.
11. Shao X, Liu J, Cao H, Shen C, Wang H. Robust dynamic surface trajectory tracking control for a quadrotor UAV via extended state observer. *International Journal of Robust and Nonlinear Control* 2018; 28(7): 2700–2719.
12. Liu K, Wang R, Zheng S, Dong S, Sun G. Fixed-time disturbance observer-based robust fault-tolerant tracking control for uncertain quadrotor UAV subject to input delay. *Nonlinear Dynamics* 2022; 107(3): 2363–2390.
13. Mechali O, Xu L, Huang Y, Shi M, Xie X. Observer-based fixed-time continuous nonsingular terminal sliding mode control of quadrotor aircraft under uncertainties and disturbances for robust trajectory tracking: Theory and experiment. *Control Engineering Practice* 2021; 111: 104806.
14. Wang X, Sun S, Kampen vEJ, Chu Q. Quadrotor fault tolerant incremental sliding mode control driven by sliding mode disturbance observers. *Aerospace Science and Technology* 2019; 87: 417–430.
15. Jia J, Guo K, Yu X, Zhao W, Guo L. Accurate high-maneuvering trajectory tracking for quadrotors: A drag utilization method. *IEEE Robotics and Automation Letters* 2022; 7(3): 6966–6973.
16. Faessler M, Franchi A, Scaramuzza D. Differential flatness of quadrotor dynamics subject to rotor drag for accurate tracking of high-speed trajectories. *IEEE Robotics and Automation Letters* 2017; 3(2): 620–626.
17. Moeini A, Lynch AF, Zhao Q. Exponentially Stable Motion Control for Multirotor UAVs with Rotor Drag and Disturbance Compensation. *Journal of Intelligent & Robotic Systems* 2021; 103(1): 1–17.
18. Cui L, Zhang R, Yang H, Zuo Z. Adaptive super-twisting trajectory tracking control for an unmanned aerial vehicle under gust winds. *Aerospace Science and Technology* 2021; 115: 106833.
19. Bhale P, Kumar M, Sanyal AK. Finite-time stable disturbance observer for unmanned aerial vehicles. In: 2022 American Control Conference (ACC). ; 2022: 5010–5015.
20. Sanyal A. Discrete-time data-driven control with Hölder-continuous real-time learning. *International Journal of Control* 2022; 95(8): 2175–2187.

21. Rosier L. Homogeneous Lyapunov function for homogeneous continuous vector field. *Systems & Control Letters* 1992; 19(6): 467–473.

22. Guo BZ, Zhao Zl. On the convergence of an extended state observer for nonlinear systems with uncertainty. *Systems & Control Letters* 2011; 60(6): 420–430.

23. Moreno JA, Osorio M. Strict Lyapunov functions for the super-twisting algorithm. *IEEE transactions on automatic control* 2012; 57(4): 1035–1040.

24. Xia Y, Zhu Z, Fu M, Wang S. Attitude tracking of rigid spacecraft with bounded disturbances. *IEEE Transactions on Industrial Electronics* 2010; 58(2): 647–659.

25. Bhat SP, Bernstein DS. A topological obstruction to continuous global stabilization of rotational motion and the unwinding phenomenon. *Systems & control letters* 2000; 39(1): 63–70.

26. Chaturvedi NA, Sanyal AK, McClamroch NH. Rigid-body attitude control. *IEEE control systems magazine* 2011; 31(3): 30–51.

27. Viswanathan SP, Sanyal AK, Samiei E. Integrated guidance and feedback control of underactuated robotics system in SE (3). *Journal of Intelligent & Robotic Systems* 2018; 89(1): 251–263.

28. Liu L, Wang D, Peng Z. State recovery and disturbance estimation of unmanned surface vehicles based on nonlinear extended state observers. *Ocean Engineering* 2019; 171: 625–632.

29. Wang N, Sanyal AK. A Hölder-continuous extended state observer for model-free position tracking control. In: IEEE. ; 2021: 2133–2138.

30. Wang N, Sanyal AK. A Hölder-continuous Extended State Observer for Rigid Body Attitude Dynamics. *IFAC-PapersOnLine* 2022; 55(22): 340–345.

31. Vidal PV, Nunes EV, Hsu L. Output-feedback multivariable global variable gain super-twisting algorithm. *IEEE Transactions on Automatic Control* 2016; 62(6): 2999–3005.

32. Sanyal AK, Bohn J. Finite-time stabilisation of simple mechanical systems using continuous feedback. *International Journal of Control* 2015; 88(4): 783–791.

33. Nordkvist N, Sanyal AK. A Lie group variational integrator for rigid body motion in SE (3) with applications to underwater vehicle dynamics. In: 49th IEEE conference on decision and control (CDC). ; 2010: 5414–5419.

34. Bhat SP, Bernstein DS. Finite-time stability of continuous autonomous systems. *SIAM Journal on Control and optimization* 2000; 38(3): 751–766.

35. Yu S, Yu X, Shirinzadeh B, Man Z. Continuous finite-time control for robotic manipulators with terminal sliding mode. *Automatica* 2005; 41(11): 1957–1964.

36. Zhu Z, Xia Y, Fu M. Attitude stabilization of rigid spacecraft with finite-time convergence. *International Journal of Robust and Nonlinear Control* 2011; 21(6): 686–702.

37. Hardy GH, Littlewood JE, Pólya G, Pólya G, others . *Inequalities*. Cambridge university press . 1952.

38. Cruz-Zavala E, Moreno JA, Fridman LM. Uniform robust exact differentiator. *IEEE Transactions on Automatic Control* 2011; 56(11): 2727–2733.

39. Chen CT. *Linear system theory and design*. Saunders college publishing . 1984.

40. Hamrah R, Sanyal AK. Finite-time stable tracking control for an underactuated system in SE (3) in discrete time. *International Journal of Control* 2022; 95(4): 1106–1121.

41. Bohn J, Sanyal AK. Almost global finite-time stabilization of rigid body attitude dynamics using rotation matrices. *International Journal of Robust and Nonlinear Control* 2016; 26(9): 2008–2022.

42. Sanyal A, Nordkvist N, Chyba M. An almost global tracking control scheme for maneuverable autonomous vehicles and its discretization. *IEEE Transactions on Automatic control* 2010; 56(2): 457–462.

43. Khalil HK. Nonlinear systems third edition. *Patience Hall* 2002; 115.

44. Pounds P, Mahony R, Corke P. Modelling and control of a large quadrotor robot. *Control Engineering Practice* 2010; 18(7): 691–699.